# TALLINNA TEHNIKAÜLIKOOL
# TALLINN UNIVERSITY OF TECHNOLOGY

## Department of Materials and Environmental Technology

# INVESTIGATION OF MORPHOLOGY AND COMPOSITION OF $Cu_2ZnSnS_4$ THIN FILMS PREPARED BY PULSED LASER DEPOSITION

## PLD MEETODIL SADESTATUD $Cu_2ZnSnS_4$ KILEDE STRUKTUURI JA KOOSTISE UURIMINE

## MASTER THESIS

| | |
|---|---|
| Student | Ge Xin |
| Student code | A156306 |
| Supervisors | Dr. Valdek Mikli; Dr. Sergei Bereznev |
| | senior researchers of the Institute of Materials and Environmental Technology |

Tallinn, 2017

## AUTHOR'S DECLARATION

Hereby I declare, that I have written this thesis independently.

No academic degree has been applied for based on this material.

All works, major viewpoints and data of the other authors used in this thesis have been referenced.

"......." .................... 201…..

Author: ..............................

/signature /

Thesis is in accordance with terms and requirements

"......." .................... 201….

Supervisor: …........................

/signature/

Accepted for defence

"......."....................201… .

Chairman of theses defence commission: ...........................................................................

/name and signature/

# LIST OF ABBREVIATIONS AND ACRONYMS

CIGS          $Cu(In,Ga)Se_2$

TCO          Transparent conducting oxide

a-Si:H          Hydrogenated amorphous silicon

RF          Radio Frequency

CSS          Close Space Sublimation

PLD          Pulsed Laser Deposition

PVD          Physical Vapor Deposition

SEM          Scanning Electron Microscopy

EDX          Energy - Dispersive X-ray spectroscopy

SKP          Scanning Kelvin Probe

SE          Secondary Electrons

BSE          Back-Scattered Electrons

# TABLE OF CONTENTS

# Acknowledgements

# INTRODUCTION

Nowadays, fossil fuels are still the main source of energy. International Energy Agency report indicated that coal, oil and natural gas accounted for 80% of total primary energy supply by fuel in 2015. However, fossil fuels are not renewable. The use of fossil fuels bring the energy crisis which has seriously affected economic and environment development. In recent year, the environmental issues such as greenhouse effect and smog have got the world's attention. In response to this condition, many countries have to adjust the energy production structure, such as reducing the use of coal and vigorously developing sustainable energy. Environment-friendly and sustainable green energy plays the important role in energy field. Solar energy, hydro power, nuclear, wind power and other resources were regarded as well alternative energy. At present, world energy structure is dominated by fossil energy and renewable energy co-exist. This energy structure will continue for a long time. However, from high-carbon conventional energy to low-carbon new energy sources is an inevitable trend.

 Solar power has developed for a long time. The source is free, durable and non-toxic. The process of using solar energy include collect, convert and save radiation energy. Photovoltaic is the key of conversion, which using the photovoltaic effect in the semiconductor to achieve conversion of light energy to electrical energy. Most of the first and second generation solar cells have achieved over 20% conversion efficiency. Emerging solar cells efficiency is less than 13%. CZTS is one of the emerging solar cells, its efficiency has achieved 12.6%. In the current study, CZTS is not efficient compared with Si, CIGS, CdTe, etc. However, its abundant elements, non-toxic and low cost make it becomes the promising solar cell. There are different physical and chemical methods were used for depositing the CZTS thin film.

This thesis is concentrated on investigation of morphology and composition of CZTS thin films prepared by pulsed laser deposition. Special attention is paid to study of the effect of temperature and selenization treatment on structure and composition of the CZTS films.

# 1. LITERATURE OVERVIEW

## 1.1 Photovoltaic basics

The photovoltaic effect is used to convert the energy of visible light into electrical energy. The first observations were performed by French physicist A. E. Becquerel in 1839 [1, 2]. Photovoltaic effect is based on semiconductivity - the conductivity of semiconductor between conductor and insulator. When electron is excited by absorbing energy, it can be excited up to the conduction band from the valence band and this process results in a hole in the valence band and an electron in the conduction band. In intrinsic semiconductor which is a kind of pure semiconductor without any dopant, the number of excited electrons are equal to holes. A semiconductor with electron concentration larger than hole concentration is called n-type semiconductor. It is formed by doping an intrinsic semiconductor with donor impurities. For n-type semiconductors the Fermi level is above the intrinsic Fermi level and close to the conduction band. In the case of p-type semiconductor, holes are the majority carries and electrons are minority carriers. P-type semiconductor can be prepared by adding of acceptor impurities to intrinsic semiconductor material. For p-type semiconductors the Fermi level is below the intrinsic Fermi level and close to the valence band.

In the solar cell, n-type semiconductor is contacted with p-type semiconductor, the carrier concentration difference between p-type and n-type leads to diffusion, electrons move from n-type semiconductor to p-type semiconductor and form a depletion region with no mobile carriers. When the sunlight is focused on the p-n junction, electrons are excited to produce free electrons which moved toward n-type area and holes which moved to p-type region. If the wire will be connected to the back contact and the p-n junction, current will be generated in circuit.

In order to better understand electronic behavior, the equivalent circuit of a solar cell is shown in **Fig.1.1.** It consists of a current source in parallel with a diode, a series resistor and a shunt resistor. The current source provides the generation of charge carriers when solar cell is exposed to light. A portion of the current flow through the diode, in this case, diode is in a forward-bias state. The series resistor represents the loss that is caused by electrode contact and the material resistivity. The shunt resistor is due to leakage current. From circuit diagram

illustrates the relationship between output current $I$, photogenerated current $I_C$, diode current $I_D$ and shunt current $I_{SH}$. ($I = I_C - I_D - I_{SH}$.)
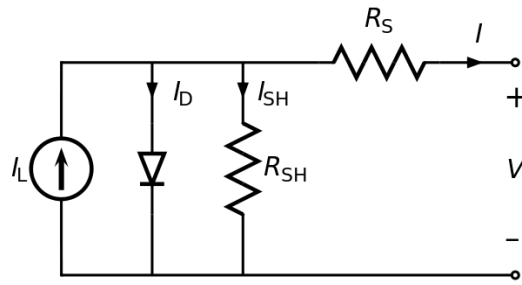


**Fig.1.1.** Equivalent circuit of a solar cell [3]

There are some parameters used to evaluate the performance of solar cells: efficiency $\eta$, open circuit voltage $V_{OC}$, short circuit current $I_{SC}$, and fill factor $FF$. These parameters can be obtained from I-V curve (**Fig.1.2**).
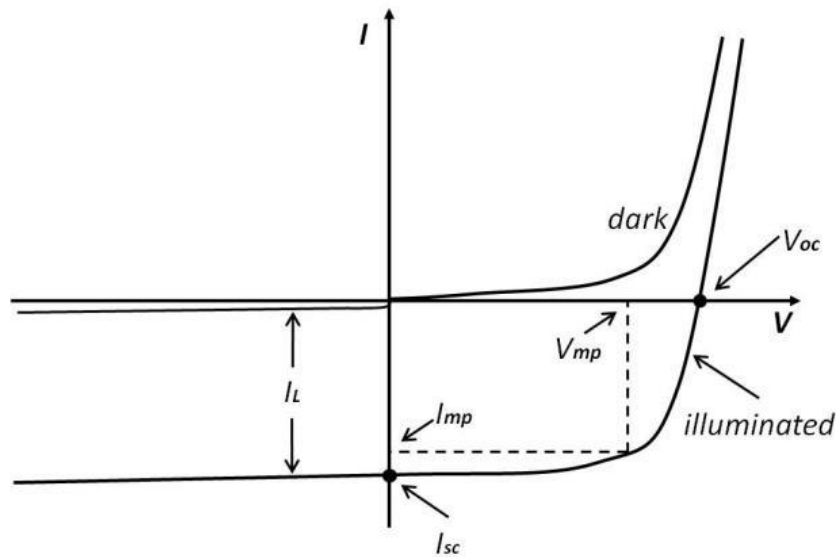


**Fig1.2** I-V characteristics of an ideal diode solar cell when non-illuminated (dark) and illuminated [4]

The fill factor is the ratio of maximum power ($P_{mp}$) to the product of open circuit voltage ($V_{oc}$) *and* short circuit current ($I_{sc}$) values, given by Eq. (1.1.1). Higher shunt resistance ($R_{SH}$) and lower series resistance ($R_S$) result in a higher fill factor. The efficiency of solar cells is the

ratio of maximum power $(P_{mp})$ delivered by the total power of light illumination $(P_{in})$ on the cell, Eq.(1.1.2).

$$FF = \frac{I_{mp} \cdot V_{mp}}{I_{SC} \cdot V_{OC}} \qquad (1.1.1)$$

$$\eta = \frac{P_{mp}}{P_{in}} = \frac{I_{SC} \cdot V_{OC} \cdot FF}{P_{in}} \qquad (1.1.2)$$

## 1.2 Structure of thin film solar cells

Substrate configuration and superstrate configuration are two typical configurations for thin film solar cells. The main difference is the stacking sequence of layers. **Fig.1.3 (a)** shows a Cu(In,Ga)Se$_2$ (CIGS) substrate cell, molybdenum (Mo) coating on a glass as the contact, p-type CIGS absorber layer is deposited on the Mo/glass contact and sequentially deposited a n-type CdS, intrinsic ZnO and transparent conducting oxide (TCO). The light illumination comes from TCO side. In the CdTe superstrate design, shown in **Fig.1.3 (b)**, n-type CdS is deposited on a transparent conducting oxide (TCO) coated glass. Then, followed by p-type CdTe absorber layer and contact. The light enter the cell through the glass.



(a)                                 (b)
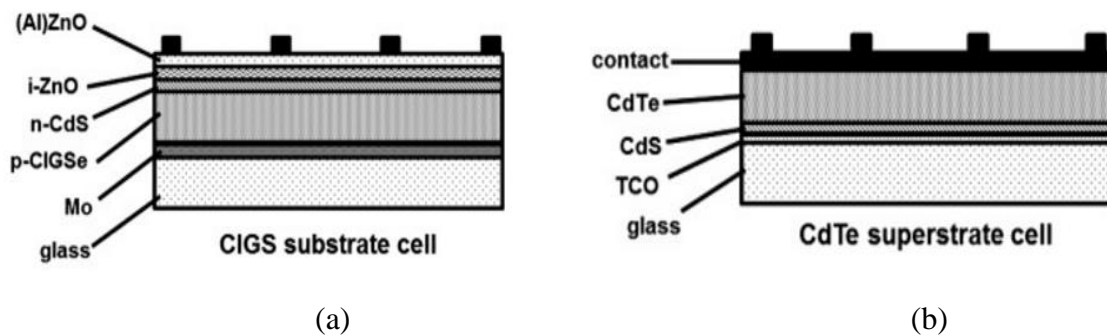
**Fig.1.3** Examples of the substrate (a) and superstrate (b) configurations used for thin film solar cells [5]

Window layer is made of high bandgap materials to avoid photogenerated carriers absorption. In order to reduce series resistance and improve the short circuit current density, window layer thickness should be as thin as possible. Buffer layer has n-type of conductivity to form p-n junction with absorber layer. It requires minimum absorption loss so that as much light as

possible reaches the absorber layer. Absorber layer is used for light absorption and for the generation of the photo-generated carriers. Back contact provides electrical contact to the back side of the film.

## 1.3 Solar cell materials

The first generation solar cells are based on crystalline silicon, it includes monocrystalline silicon and polycrystalline silicon. Nowadays, crystalline silicon with its mature development and good performance dominates the solar cell market. Thin film solar cell is the second generation. Compared with the first generation, it reduces the consumption of materials and achieves low production costs. The typical materials in this category are amorphous silicon, CdTe and CIGS.

The solar cell efficiency is shown in **Fig.1.4**. In order to improve conversion efficiency of solar cell, concentrator and multi-junction structure are applied in PV cell. Concentrating optics used to focus the sunlight on small cells by lenses and curved mirrors, results in the significantly increased radiation intensity of the light absorbed by the cell . For multiple materials, each material can respond to light wavelength due to its multiple bandgaps. So it can capture more energy to avoid the loss of energy. The maximum theoretical efficiency of single-junction cells is 33.16 % [6] . However, an infinite number of junctions theoretical value up to 86.8 % under highly concentrated sunlight [7] is available.

In fact, produce multiple materials is not an easy task because the electrical characteristics of each layer has to be carefully matched. III-V compound semiconductors have good performance in this field.
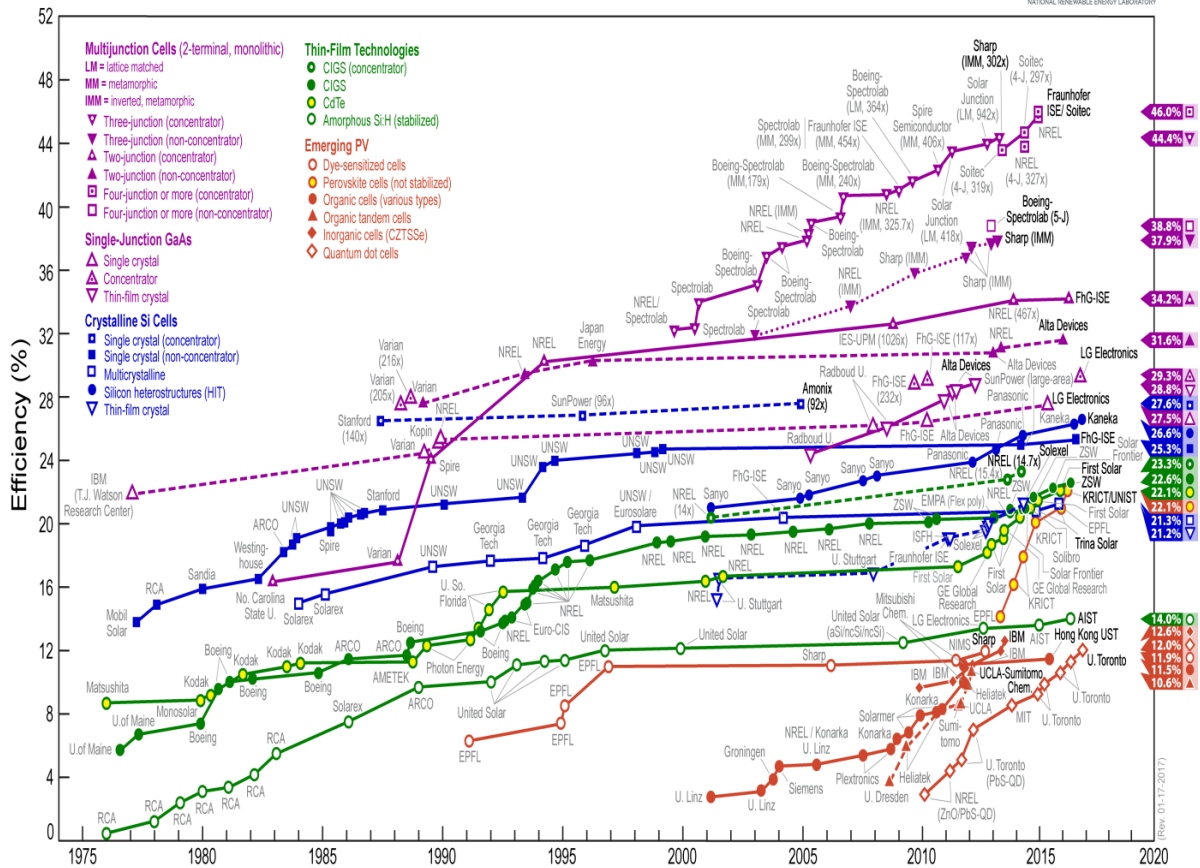
**Fig.1.4** Achieved efficiencies of the different solar cells [8].

In 2004, German Fraunhofer Institute for Solar Energy Systems ISE, French Soitec and CEA-Leti (Laboratory of Electronics Information Technology) have achieved a world record conversion efficiency of 46.0 % for a four - junction GaInP/GaAs//GaInAsP/GaInAs solar cell. This cell was based on III-V compound semiconductors and used in concentrator photovoltaic system. Single junction GaAs has efficiency of 27.5 % and 29.3 % if using concentrator. Conventional solar cell possesses nowadays the efficiency between 20 % to 30 %, which include crystal silicon, amorphous silicon, CdTe and CIGS. Besides, emerging solar cells such as organic cells, dye-sensitized cells and CZTSSe based cells are relatively inefficient (10 %-13 %)..

Ideal absorber materials require band gap between 1.0 - 1.5 eV, high optical absorption $10^4$-$10^5$ cm$^{-1}$ in the wavelength region of 350-1000 nm, low recombination velocity, high quantum yield for the excited carriers and long diffusion.[9] **Fig.1.5** shows bandgaps of the different

semiconductors. With proper band gap, Si, a-Si, GaAs, InP, CIGS and CdTe have been used as absorber layer for photovoltaic cells. The band gap of CdS is 2.42 eV, it can be used as window-buffer layer in thin film solar cells.
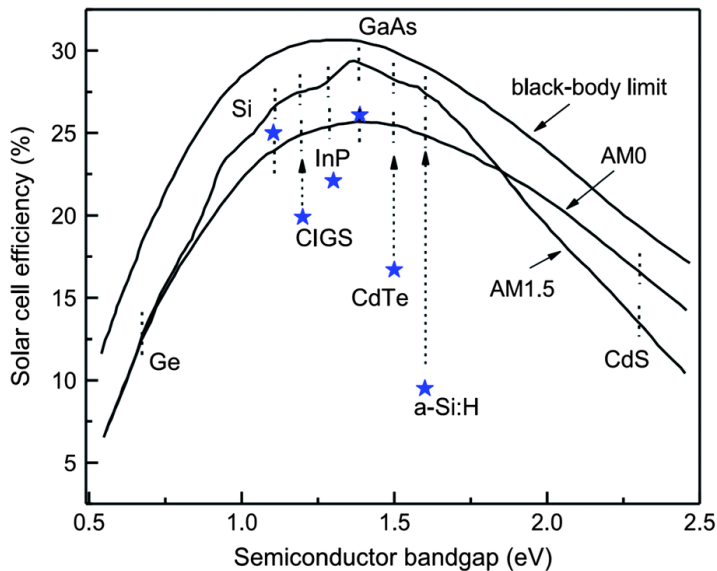


**Fig.1.5** Power conversion efficiency as a function of semiconductor band gap [10]

### 1.3.1 Crystal Silicon

In the present time crystal silicon wafer covers in PV production over 90 %. There are two types of photovoltaic technologies based on crystalline silicon : monocrystalline and polycrystalline.

Monocrystalline silicon has the longest development and silicon technology is the most mature technology of solar cell. Monocrystalline silicon has regular atomic arrangement and it is free of grain boundaries. So it is the most efficient silicon material. The maximum efficiency what is reached in the lab is 25.3 %.(see, **Fig.1.4)**

Single crystal of silicon is grown from cylindrical ingots, e.g. by Czochralski growth process. Dipping seed crystal into the high purity molten poly-silicon at 1425 °C. Pulling the seed upwards and simultaneously rotating the monocrystalline silicon can form up to an ingot size of 200-300 mm diameter and 2 meter length. Silicon wafer is made by cutting cylindrical ingot and then assembling them into modules. Monocrystalline silicon solar panels are the

most expensive type of solar panels. On the one hand, it requires high purity silicon. In addition, cutting off four sides of single crystal for fabrication of cell wafer causes large amount waste of the material. Therefore the cheaper polycrystalline and amorphous silicon materials have been investigated and used in solar cells.

Polycrystalline silicon is another option for production of the crystalline silicon PV cell. There are grain boundaries in polycrystalline silicon, which decrease the electrical and thermal conductivity of the material. In solar cells, grain boundaries affect conversion efficiency by limiting carrier flows and allowing extra energy levels in the forbidden band. As a result the recombination rate increases. To avoid recombination, the grain size needs to be on the order of a few millimeters [11]. The record lab cell efficiency is 21.3 % for polycrystalline silicon.

Compared with monocrystalline silicon, lower cost provide a significant advantage. Polycrystalline silicon technology is relatively simpler than that of single crystal silicon - small silicon crystals are melted and poured in the the molten form into a square cast followed by recrystallization. Next step is cutting into the wafers. The efficiency of polycrystalline silicon is lower than the efficiency of monolystalline silicon. Thus, the panel needs more surface to produce electrical output. Another disadvantage is slightly worse performance in high temperature conditions than monocrystalline due to its lower heat tolerance.


**1.3.2 Amorphous silicon**


Amorphous silicon lacks long-range order in the structural arrangement of the atoms, so some atoms have a dangling bond. This defect will affect electrical behavior. Nevertheless, passivation of these dangling bonds by hydrogen can improve the quality of materials. However, this material can cause the Staebler‑Wronski effect - the defect density increases with light exposure, resulting in a reduction in conversion efficiency [12]. The highest achieved lab efficiency in thin-film amorphous silicon solar cells is 14 %.

Hydrogenated amorphous silicon (a-Si:H) can be used for thin film solar cells. Light weight and low cost make it competitive in the photovoltaic market. The film can be deposited on a variety of flexible substrates. Lower efficiency is a problem for hydrogenated amorphous silicon, so the real application of a-Si:H for energy conversion is small. Typical amorphous

silicon cell adopts p-i-n structure, thin film is deposited on glass by chemical vapor deposition technology. Stacked multilayer a-Si film can increase efficiency.

### 1.3.3 CdTe

Cadmium telluride is the II-VI semiconductor. CdTe has appropriate direct band gap of 1.45 eV, high absorption coefficient, high chemical stability and relatively low cost. Due to these advantages, it has been considered as a very promising material for solar cells [13]. The main reason for cells inefficiency is defects in CdTe, including dislocations, grain boundaries and interfaces - they cause the increase of the recombination rate. Nevertheless, post-growth treatments can improve the efficiency, for instance, typically the heat treatment in the presence of $CdCl_2$. Recently, company First Solar announced the CdTe cell conversion efficiency of 22.1 %. However, it still did not reach the theoretical limit of 32 % [14]. In 2014, increase of module efficiency from 16.1 % to 17.0 % was achieved [15].

Constituent elements cadmium and tellurium make the CdTe material toxic, especially Cd. So the toxicity  raised concerns about environmental issues. The release of toxic substances will have a serious impact. There is no definite conclusion on this issue [16, 17]. Fortunately, the crystalline lattice of CdTe has good chemical stability. Related records proved that is no cadmium release from CdTe PV module during fire [18, 19]. Moreover, superstrate configuration as environmentally more safe structure has higher efficiency than substrate configuration for CdTe.

### 1.3.4 CIGS

Copper indium gallium diselenide is an I-III-VI$_2$ semiconductor with chalcopyrite crystal structure. It has an adjustable band gap from 1.0 eV to 1.7 eV and high coefficient over $10^5$ cm$^{-1}$ for 1.5 eV [20]. It was reported that the highest lab efficiency is 22.6 % in 2016 [21].

Thickness of 1.2-4 µm can meet the production needs. Compared with crystal silicon 70‑200 µm, CIGS reduces the use of materials. The common method of fabricating CIGS absorber layer is to co-evaporate or co-sputter copper, gallium and indium onto a substrate and anneal the stack in selenium vapors.

### 1.3.5 GaAs

The first GaAs heterostructured solar cells was produced in 1970. GaAs is an III-V semiconducting compound with zinc blende crystal structure. It has a wide and direct band gap of 1.42 eV, so GaAs can absorb more photons efficiently. High efficiency, low temperature coefficient and strong light performance make it the promising candidate for the absorber in solar cells. Single junction GaAs thin films held a record efficiency of 28.8% [22], which is the highest conversion efficiency in thin film-type solar cells. In addition, GaAs solar cells are extensively used in space applications and concentrated photovoltaic systems. A major problem of GaAs cells is that the material itself is expensive.

### 1.3.6 $Cu_2ZnSnS_4$

CZTS is an $I_2$-II-IV-$VI_4$ quaternary p-type semiconducting compound with kesterite structure. In the first report about CZTS by Nitsche et al [23] the iodine vapor transport method was used to fabricate single-crystal CZTS. CZTS has been regarded as a promising absorber layer material in the thin film solar cells due to its excellent properties: optical band gap 1.5 eV, high absorption coefficient more than $10^4$ $cm^{-1}$ in the visible light region as well as the chemical elements are low cost, non-toxic and abundant in the earth crust [24]. The record lab cell efficiency has been achieved as 12.6 % on a 0.42 $cm^2$ substrate.
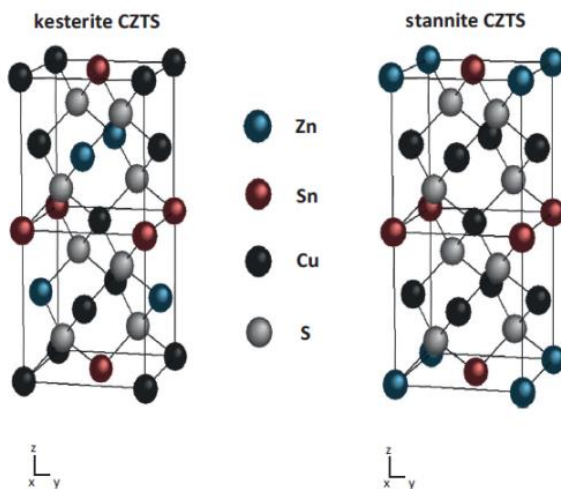


**Fig.1.6** Crystal structure of CZTS [25]

In order to obtain CZTS, In (or Ga) atom is replaced by Zn and Sn atom in the $Cu(In,Ga)(Se)_2$ structure. **Fig.1.6** shows two crystal structures of CZTS - Kesterite and Stannite. The difference between structures is the arrangement of Cu and Zn. By contrast, Kesterite structure is more stable than Stannite structure due to lower energy. However, kesterite and stannite structure are very close in energy and they may coexist in the synthesized samples at room temperature.

Ternary phase diagram of the $Cu_2S$-ZnS-$SnS_2$ system illustrates that CZTS can be grown only in a very narrow region **(Fig.1.7)**, and secondary phases can be formed very easily. Therefore, it is difficult to deposit single phase CZTS without secondary phases. ZnS, SnS, CuS, and $Cu_2SnS_3$ are common additional phases in CZTS. These phases have large effect on the efficiency of CZTS cells, because they provide the shunt current paths and recombination centers for electron-hole carriers. Moreover, it is easy to form point defects due to the similar radii of the various ionic species [26]. The earlier report [27] shows that high efficient solar cell should be copper-poor and zinc-rich. This is because the Cu-poor composition promotes the formation of Cu vacancies, which are shallow acceptors, while the Zn-rich composition inhibits the substitution of Cu in the Zn sites, which are deep acceptors [28].
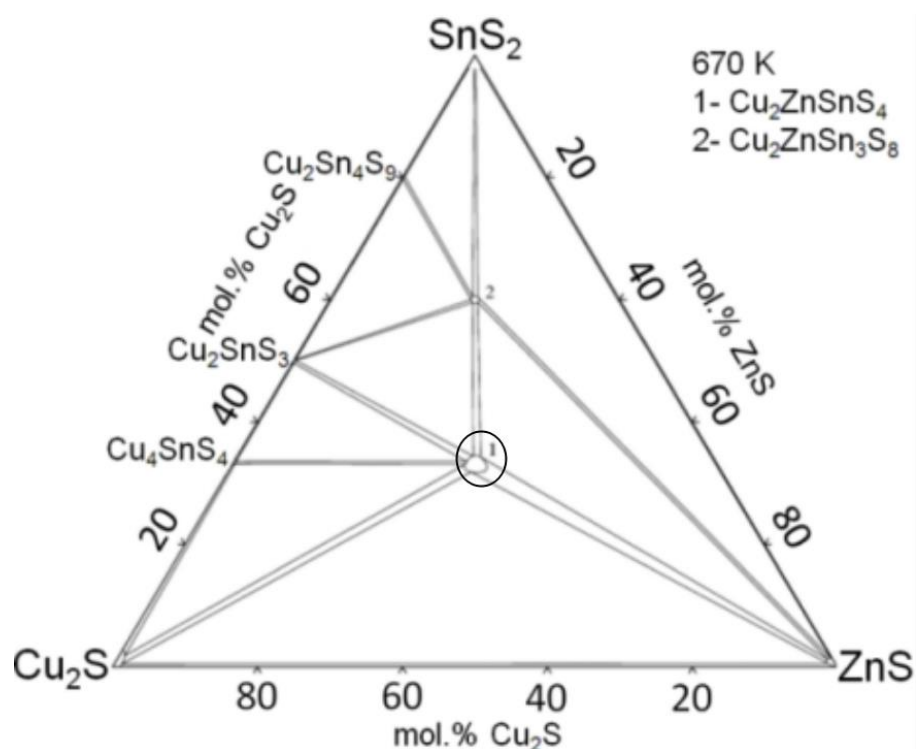


**Fig.1.7** Phase diagram of $SnS_2$-$Cu_2S$-ZnS system [29]

## 1.4 Methods for thin films for solar cells preparation

Thin films can be deposited with a variety of physical and chemical techniques. For instance, RF magnetron sputtering [30, 31], chemical bath deposition [32, 33], sol-gel sulfurizing method [34], spray pyrolysis [35, 36], pulsed laser deposition [37, 38], thermal evaporation [39, 40], atom beam sputtering [41] and electrodeposition [42, 43].

### 1.4.1 RF magnetron sputtering

Radio frequency magnetron sputtering is a physical vapor deposition method, it can be used to make high quality films at low temperature using different substrates. In the magnetron sputtering arrangements, the magnetic field parallel to the target. And the electric field perpendicular to the magnetic field. As a result, the sputtering rate increases due to increased concentration of plasma and enhanced ion collision. Compared with DC magnetron sputtering, radio frequency magnetron sputtering can be applied to insulators.

The principle of RF magnetron sputtering is shown in **Fig1.8.** Sputtering process is working in vacuum system. In the effect of electric field, electrons collisions with argon atoms lead to ionization. Generated Ar+ ions are accelerated to move to the target and bombard the target surface with high energy, resulting in sputtering of the target material. In the sputtered particles, a neutral target atom or molecule is deposited on the substrate to form a thin film. Driven by the magnetic field and the electric field, the resulting secondary electrons drift in the specified direction. In case of toroidal magnetic field, the electrons do circular motion on the target surface. Their motion paths is very long and bound to the plasma area near the target surface. So that a large amount of Ar+ ions are ionized in the region to bombard the target, and a high deposition rate is achieved. As the number of collisions increases, the energy of the secondary electrons is exhausted, gradually away from the target surface, and eventually deposited on the substrate. Due to the low energy of the electrons, the energy delivered to the substrate is small, resulting in substrate temperature is slowly increasing.
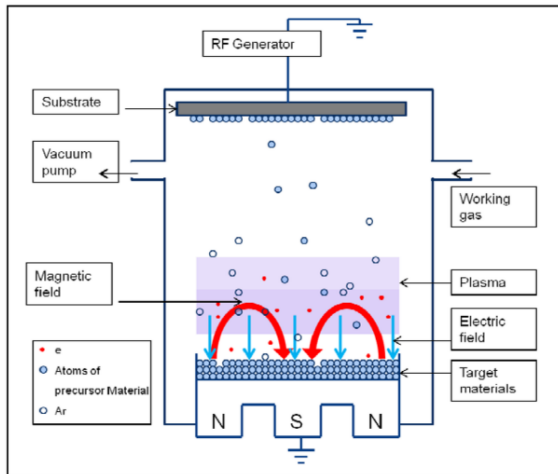
**Fig.1.8** Schematic representation of RF magnetron sputtering [44]

## 1.4.2 Close space sublimation

Close space sublimation is mainly applied in deposition of CdTe films. Based on this technique, the efficiency of CdTe solar cells is relatively high. A schematic diagram is shown in **Fig.1.9.** The apparatus includes two heaters, upper and below graphite pieces, substrate and CdTe powdered target.
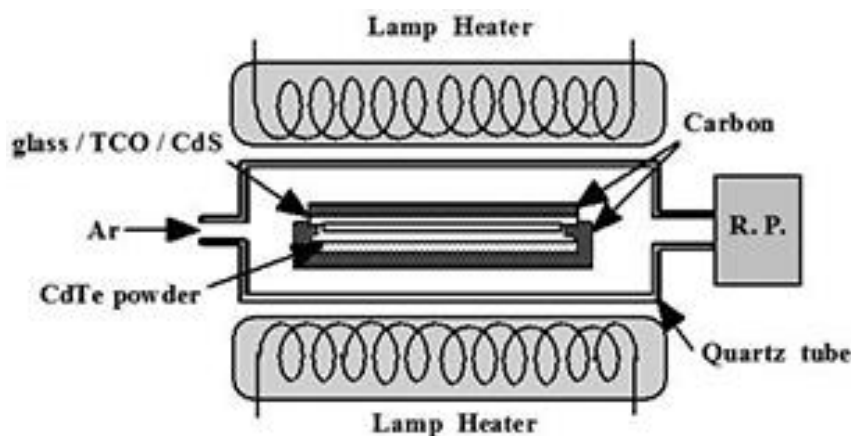


**Fig.1.9** Schematic view of close space sublimation (CSS) apparatus [45]

The evaporation source is placed in a holder having the same area as the substrate. When the temperature exceeds 400 °C, CdTe sublimates and partially decomposes. Re-evaporation of Cd and Te from the growing CdTe surface limits the deposition rate and utilization. At higher total pressure, about 1Torr, this problem can be optimized, but mass transfer from the source to the substrate becomes diffusion-limited.[46] Thus, the substrate and source should be as

close as possible. The proximity of the substrate and the source can reduce the temperature difference between the two so that the film grows in an ideal state. If CdTe is deposited on a lower temperature substrate, it will form a polycrystalline thin film. In order to obtain a high quality film, pressure, substrate temperature and source temperature should be considered.

### 1.4.3 Chemical bath deposition

Chemical bath deposition is a simple, inexpensive technology for deposition thin films. It can be applied to large-scale and continuous deposition. Substrate is immersed in precursor solution and thin film is deposited on substrate due to nucleation and particle growth, often without any subsequent heat treatment. Using this method stable, uniform, adherent and hard films can beobtained.[47]

Bath temperature, concentrations of precursors in solution, pH of solution and deposition time have an effect on growing films. Increasing the bath temperature can promote diffusion, ionic mobility and crystalline growth, hence reasonable control of the temperature to improve the quality of the films. The bath temperature is below 100 °C,  so the materials do not need to tolerate high temperature. Thus, materials have a wide range of options. One of the disadvantages of this method is the wastage of precursor solution after every deposition.

### 1.4.4 Spray pyrolysis

The first introduction of the spray pyrolysis technique was reported by Chamberlin and Skarman in 1966 [48]. Spray pyrolysis is a versatile technique that can be used for deposition of films and for powder production. The scheme of spray pyrolysis is shown in **Fig.1.10.** Spray pyrolysis equipment consists of spray solution, atomizer, substrate and temperature controller. Metal salt solution is atomized by atomizer and sprayed on the heated surface. In this process, aerosol is generated and transported to heated substrate. After solvent evaporation, the film is deposited on the substrate and drying and decomposition of precursors take place.
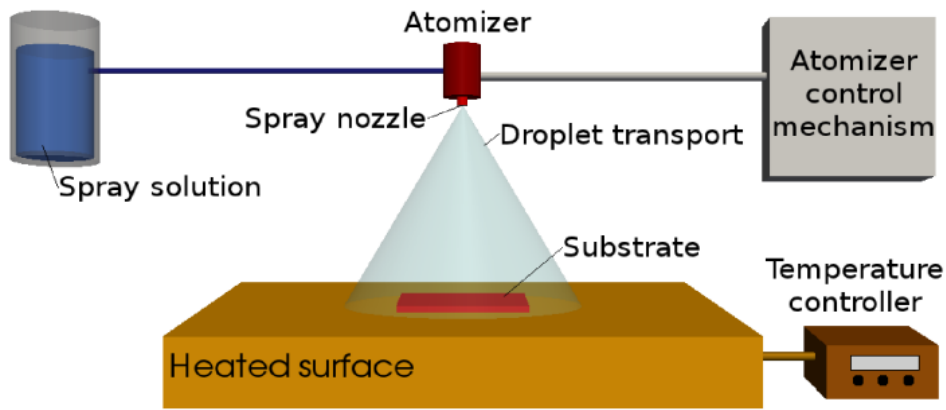
**Fig.1.10** General schematic drawing of a spray pyrolysis deposition process [49]

The temperature of the substrate surface is the most important spray pyrolysis parameter, which determines the morphology and properties of the film. As the temperature increases, the film morphology can change from cracks to porous microstructures. The precursor solution is another factor that affects the growth of the film. The physical and chemical properties of the precursor solution are affected by solvent, salt type, salt concentration and additives. Thus, changing the composition of the precursor solution can control the structure and properties of the deposited film.

## 1.4.5 Pulsed Laser deposition

Pulsed Laser deposition (PLD) is a physical vapor deposition (PVD) technique, which is applied in the production of high-quality films. The schematic diagram of PLD is illustrated in **Fig.1.11**. Basically, a high-power pulsed laser beam is used for ablation onto a rotating target within a vacuum chamber. The target surface is struck by a high energy beam which results in the breakdown of chemical bonds. Thus, the material on the target surface area is vaporized forming a plasma plume which consists of electrons, ions, atoms, molecules, clusters, particulates and molten globules. The plasma plume expands rapidly away from the target surface, the particles stick to the substrate with high adhesion and are compressed as the film. The process can be carried out in ultrahigh vacuum or in the background gas according to the type of deposited films. For example, when depositing the oxides, in order to completely oxidize the deposited films, oxygen is usually selected as the background gas.
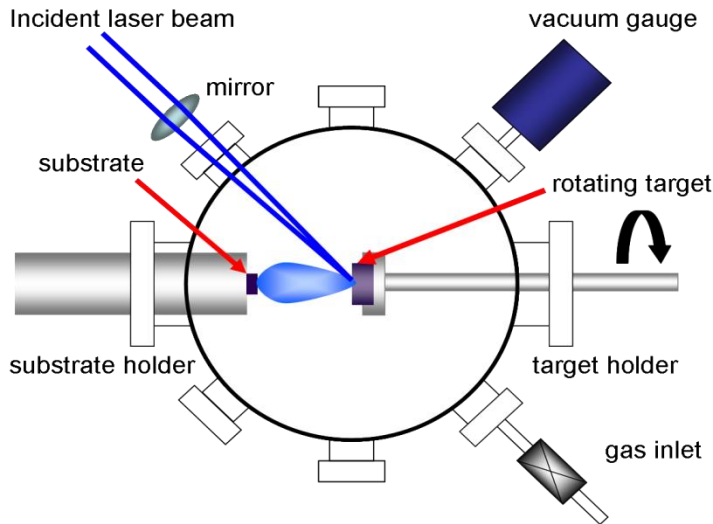
**Fig.1.11** Schematic view of a PLD system [50]

Compared with many other deposition techniques, the PLD is relatively simple but accompanied by a complex mechanism, which includes laser ablation of the target material, generation of a plasma with high energetic ions, electrons and neutrals. The ablated material is deposited on the substrate, followed by nucleation and the crystalline growth of the film on the substrate surface.

Several deposition parameters should be optimized for improving the quality of the films, such as laser energy density, repetition rate, laser wavelength, pulse duration, distance between the substrate and the target, pressure of the reactive background gas and substrate temperature. The temperature of the substrate is an important influential factor; the increase in substrate temperature can result in higher atom mobility, which leads to promotion of crystallization.

The most attractiveness of PLD technique is the stoichiometric transfer. It means that the deposited films can be obtained with the same composition as the targets, so the composition of the film is controlled precisely by making the desired composition target. This advantage enables the growth of complex multicomponent materials. PLD can be used in production of a wide range of materials, such as metals, semiconductors, oxides, fluorides, borides, carbides, nitrides, silicides and sulfides. Nevertheless, thermally sublimable materials, easily evaporated metals, and toxic materials are not suitable for processing by this technique. In addition, the deposition process is extremely clean as a result of the placement of the laser source outside the reaction chamber.

Particulates are easily formed in growing film process, which have an impact on performance of films. In general, high-performance optical and electronic applications need to minimize particulates density and size as much as possible by means of selecting the appropriate operating parameters. The particulates are ejected from target in the form of solid, liquid or vapor. From the aspects of size, particulates formed from the vapor state tends to be in the nanometer range, while formed from the liquid or solid state tends to be in the micron and submicron range. In terms of shape, the particulates formed by the liquid tends to be spherical, while the particulates formed by the solid tend to be irregular. The shape of particulates formed by the vapor state tends to be spherical or polyhedral [51].

In order to improve performance of thin films, elimination of particulates is required. Preparation of homogeneous and high density target, reduction of the laser power density by increasing the spot size are the approaches to reduce the particulates production. Another approach is based on particulates velocity by reason of particulates velocity is smaller than atomic and molecular species. Adding a filter can limit the particulates and allow molecules and atoms to pass through. Moreover, using an off-axis deposition and substrate bias can also decrease particulates density in the films [52].

Preparation of thin films by PLD technology in commercial applications require large-area deposition. The first large-area films technique was achieved by using a rastered laser beam, large distance between target and substrate, a rotating substrate and a large-diameter counter rotating target. This method has been successfully applied in deposition of YBCO over 75 mm diameter substrates. The second large-area deposition is off-axis PLD, it is based on a fixed-position laser beam, the laser beam was focused close to the outer edge of rotating target and the center of rotating substrate is offset from the center of the ablation plume. Off-axis PLD has achieved the deposition of YBCO films over 50 mm diameter substrates and $Bi_4Ti_3O_{12}$ films over 100 mm diameter substrates. The third technique is rotational/ translational PLD. It utilized a static-position laser beam and a rotating substrate. The substrate translation is controlled by computer, which is back and forth in one direction. Rotation/translational PLD has been utilized to deposition of thallium-based superconducting oxides over 50 mm-diameter substrates. [53]

Uniformity is a major consideration in large-area PLD approaches. Comparison of three large-area PLD technologies: rotation/translational PLD and rastered PLD can obtain uniform composition in thin films, while off-axis method is not. In terms of the uniformity of the electronic properties, three large-area deposition technologies have a good performance. [54]

## 1.5. Aim of the Thesis

The main goals of the thesis are:

- to prepare uniform CZTS targets for PLD;

- to prepare CZTS thin films by PLD;

- to analyze structure of CZTS films by high resolution scanning electron microscopy (HRSEM);

- to analyze composition of CZTS films by energy - dispersive X-ray spectroscopy (EDX);

- to analyze photosensitivity of CZTS films by scanning Kelvin probe (SKP);

- to analyze the effect of selenization treatment on the structure and composition of CZTS films.

The main novelty of the study is in the that a special single phase CZTS target was used for PLD film depositions. The target was made from monograin CZTS powder [55] and from polycrystalline CZTS powder by sintering the powders into uniform polycrystalline targets.

# 2. Apparatus, methods and sample preparation

## 2.1 CZTS target preparation by different methods for PLD application

PLD is a method which provides material transport of the target directly to substrate. Thereby the quality of target is very important. Researchers using PLD technique for deposition CZTS films have used different methods to obtain suitable target. CZTS targets have been synthesized by mechano-chemical way or by using solid phase reactions. Some preparation methods are described below.

1. Generally the target was synthesized by heating binary compounds in a quartz ampoule. Powders of $Cu_2S$, $ZnS$ and $SnS_2$ were mixed with 1:1:1 molar ratio. The resultant powder was (shaped) pressed into a pellet and sealed into an evacuated quartz ampoule and heated in a furnace at 750 $^oC$ for 24 h. After cooling to the room temperature, the ampoule was opened and the both sides of target were polished [56-58].

2. CuS, ZnS and SnS powders were mixed in the molar ratios of Cu/Zn/Sn/S=1.6/1.3/1.1/4 for CZTS poly-crystalline sample. . Then, pressed under 5090 kg $cm^2$ mixture samples   were inserted into a pyrex tube and sealed under vacuum of $1.0 \times 10^{-3}$ Pa. The encapsulated sample was heated up to 400 $^oC$ with a ramp of 1.0 deg/min. in a furnace, held there for 1 h to ensure homogeneous reaction in solid phase, and then cooled to room temperature with ramp of 1.0 deg/min [59].

3. Cu, Zn, Sn and S powders were sealed into fused silica tubes under vacuum with argon at 1 Pa. The ampoules were heated to 650 $^oC$ at the rate of 0.5 and 2 deg/min and kept there for 48 h to get bulk CZTS. The sulphur bulk made into powders are calcined at 850 $^oC$ for 96 h. The sulfur powders and bulk CZTS  kept in a graphite box are held at 800 $^oC$ under argon pressure of 60 MPa for 5 min [60].

4. $Cu_2S$, ZnS and $SnS_2$ powders with molar ratio of 1:1:1 were mixed, pressed into a pellet and sintered at 700 °C for 4 hours in a sealed alumina tube-furnace under Ar atmosphere [61]..

## 2.2 SEM

Scanning electron microscopy is an analysis technique using of electron microscope. This technique provides the high resolution, large depth of field and three-dimensional images, making it one of the most versatile technique for analysis of solid samples (**Fig. 2.1**).

The first concept of scanning electron microscopy was described by M. Knoll in 1935, subsequently Manfred von Ardenne in 1937 invented a true microscope with high magnification by scanning a very small raster with a finely focused electron beam [62]. In fact, the first scanning electron microscope with resolving power of 50 nm was achieved in 1942. But the collection and amplification of the signal needed to be optimized. Nowadays, a purchaser has more than 40 different SEM models of choice based on a various working principles in image formation and sample analysis. Major changes have emerged with developments in computer systems and digital image storage. Field emission guns and short-focus lenses have achieved resolving powers at the sub-nanometer level [63].
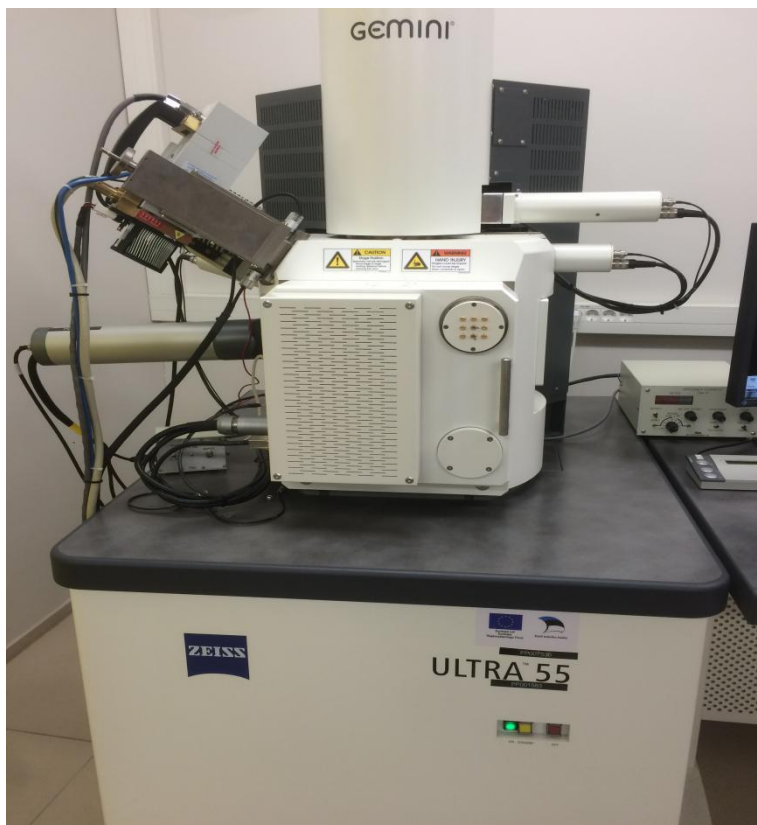


**Fig.2.1** SEM

The electron beam generated by the electron gun is accelerated and focused by lenses to a spot about 0.4-5 nm in diameter. By means of scan coil, scanning the specimen in a raster scan pattern. Interaction of the electron beam with atoms in the specimen generate various signals, include secondary electrons (SE), reflected or back-scattered electrons (BSE), photons of characteristic X-rays and light (cathodo-luminescence) (CL), absorbed current (specimen current) and transmitted electrons. These signals can be collected by specific detectors.

When the beam is accelerated to bombard the sample, they penetrate into the depth of about 1 μm and forming an interaction volume within the sample. The size of interaction volume is affected by a number of factors including: (1) atomic number, interaction volume decrease with higher atomic number, (2) accelerating voltage, interaction volume increase with higher accelerating voltage, (3) angle of incidence for the electron beam, and interaction volume decrease with higher incident angle.

Secondary electrons detection is the most common SEM mode to get information about topography of the specimen surface. Secondary electrons are generated by inelastic scattering interactions between k-shell of the specimen atoms and beam electrons. This process occurs near the specimen surface and emitted secondary electrons with low energy below 50 eV. The signal of secondary electrons provide high resolution images. Using in SEM the Shottky type cathode is combined with short-focus lenses and in-lens secondary electron detector can achieve the point resolution of 0.8 nm.

Backscattered electrons consist of over 50 eV high-energy electrons, which result from inelastic scattering interactions between specimen and beam electrons. Different atom numbers result in different number of backscattered electrons. The backscatter coefficient increases with increasing atomic number and so higher atomic number elements will appear brighter than low atom number elements in the image [60]. Thus, BSE are used to detect composition contrast. Nowadays SEM can be used in both - High vacuum ($10^{-4}$ Pa) and Low vacuum (3000 Pa) modes. High vacuum is traditionally used for inorganic materials characterization when low vacuum is reserved for life- sciences.

An additional possibility is to use SEM together with ion column (usually with Ga- ions) - so called FIB-SEM (focused ion beam SEM). It enables to perform materials etching in nanoscale and to produce very complicated structures.

## 2.3 EDX (EDS)

Scanning electron microscopy (SEM) is usually equipped μm with Energy - Dispersive X-ray microanalysis system (EDX) to analyze the chemical element composition of the material. Each element has a unique atomic structure resulting in unique peaks on its electromagnetic emission spectrum, so it is possible to analyze elements of samples using this technology.

The interaction of the electron beam with atoms causes electrons from inner shell to emit and create vacancies in the inner shell at the moment when atoms are in an excited state. In order to return atoms to the ground state, electrons have to fill vacancies from a high state and an X-ray is emitted to balance the energy difference between the high-energy shell and the lower-energy shell.

X-ray strikes the lithium drift silicon detector, it produces electron-hole in the crystal and creates a charge pulse. The charge pulse is converted to a voltage pulse, which is proportional to the X-ray energy. Subsequently, the signals are sent to the multi-channel analyzer. The spectrum of X-ray energy is evaluated to determine the elemental composition of the sample. Today the Si(Li) detectors are changed with so called silicon-drift detectors (SDD) as they can generate 100-1000 times more signal quants and additionally SDD operates at relatively "normal" temperature (-30 - -70 °C), when the Si(Li) detector needed cooling down to liquid nitrogen temperature (-196 °C).

There is a relationship between characteristic X-ray wavelength and atomic number. X-ray can be used for qualitative analysis and quantitative analysis of samples. Qualitative analysis is to find the elements present in the sample by identifying the lines in the X-ray spectrum according to energy or wavelength tables. Quantitative analysis is the measurement of the X-ray intensity by counting pulses generated in the detector. Elements from atom number 3 (Li) to 92 (U) can be detected [64, 65]

Poor energy resolution of the peaks is the limitation of EDS analysis method. In EDS analysis process, peak overlapping occurs frequently. In addition, peak overlapping or the sum of lower energy peaks also lead to produce some small peaks. The widths of X-ray peaks are determined by the energy resolution of the detector, but not by the atoms in the specimen. Typical EDS peak is about 100 times the natural peak width, which is limited by the statistics of electron-hole pair production and electronic noise, resulting in severe peak overlaps [66]. Typical sensitivity of the modern EDX system to chemical elements determination is about of

0.1 mass% (not for light elements before Na) and the quantitative determination precision can be better than 1 %.

## 2.4 Kelvin probe

Historically, the first concept of Kelvin method was presented by Lord Kelvin in 1861. The Kelvin probe is a non-contact, non-destructive analytical tool used to investigate properties of materials. It is based on a vibrating capacitor formed between a conducting specimen and a vibrating tip, which measures the work function difference or, for non-metals, the surface potential. The work function is the minimum energy required to remove an electron from the surface of conducting material to a point just outside the metal with zero kinetic energy [67]. It is an extremely sensitive indicator of surface condition and is affected by adsorption, evaporated layers, surface roughness, surface and bulk contamination, oxide layer imperfections, illumination, etc.
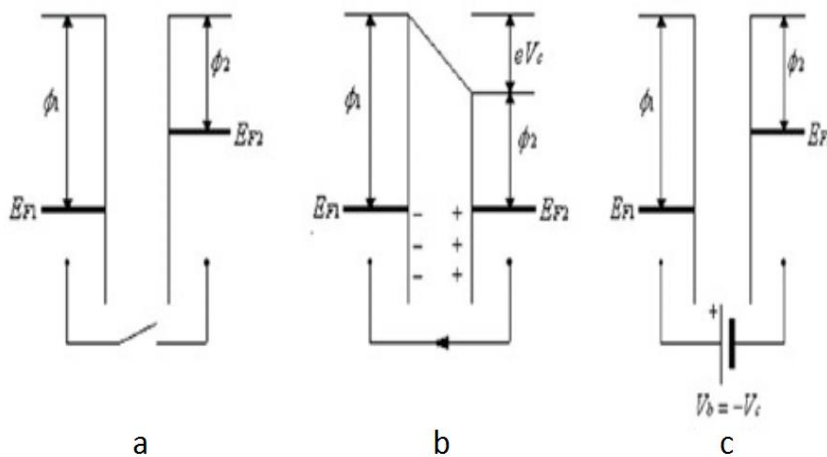


**Fig.2.2** Energy and charge diagram illustrating Kelvin probe technique principle [68]

**Fig.2.2** shows the principle of Kelvin probe technique. $\Phi_1$ and $\Phi_2$ are the work functions of materials, and $E_{F1}$ and $E_{F2}$ are the Fermi-levels. To form a capacitor, two electrodes with different work function are positioned parallel in non-contact proximity. When an external electrical contact is made between two conducing materials, the electrons will flow from the low work function to the high work function producing a contact potential $V_c$ between the materials. As a result, two surfaces have equal or opposite charges. In order to measure the

contact potential $V_c$, an external potential $V_b$ is applied to the capacitor until charges disappear, resulting in a null output voltage. At this point, $V_b = -V_c$.

In practice, a vibrating tip is utilized as a reference surface above the stationary specimen to form a capacitor. The probe tip is non-direct contact with the specimen, but rather by electrical contact. Typically the distance between the tip and the sample is about 0.2-2.0 mm. This non-contact design does not have effect on the electrical or chemical structure of the specimen. The output voltage varies periodically as the tip vibrates, and the peak-to-peak voltage depends upon the difference between the contact potential and the external voltage.

The Kelvin Probe provides a relative work function between reference surface and specimen. In order to get absolute work function $\Phi_s$, the tip work function $\Phi_{tip}$ has to be known. The tip can be calibrated by the use of photoelectric emission and *in situ* reference electrodes. Electrons are emitted from the low work function surface $\Phi_{lo}$ by a monochromatic light $E_{ph}$ ($E_{tip} > E_{ph} > E_{lo}$). And then, the tip work function $\Phi_{tip}$ and the absolute work function $\Phi_s$ of the other samples can be obtained by the formulas: $\Phi_{tip}=E_{ph} +eV_b$ and $\Phi_s=\Phi_{tip} +eV_c$. [69]

The Kelvin probe technology system provides a high work function resolution of 1- 3 meV. Standard tips of 2 and 0.05 mm in the air and anything from sharp to 10 mm in ultrahigh vacuum. The tip vibrates with amplitude of 0.1 to 1mm at a frequency of 30-300 Hz and its mean position is maintained within 50 nm.
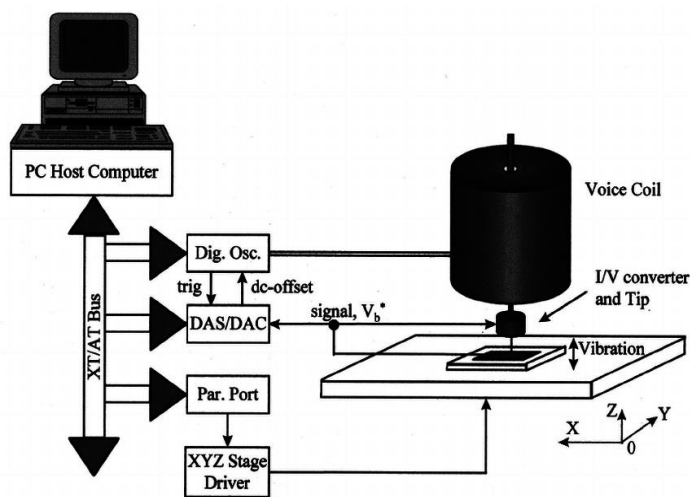


**Fig.2.3** Schematic of the scanning Kelvin probe arrangement [70]

A complete scanning Kelvin Probe system consists of a digital oscillator to drive the tip movement, a tip actuator, a signal amplifier and a scan controller. The schematic diagram of SKP arrangement is displayed in **Fig.2.3**. A digital oscillator controls the voice-coil frequency,

amplitude and probe trigger. In addition, a digital-to-analogue converter (DAC) controls a voltage source termed the backing potential ($V_b$), which cause electrical contact between the tip and the sample. A current-to-voltage converter (I/V converter) is located close to the tip. And a data acquisition system (DAS) measures the peak-to-peak output signal as a function of the backing potential $V_b$. The Sample translation is done by adjusting the XYZ stage driver.

## 2.5 Preparation of targets for PLD of CZTS films

In this work targets for PLD of CZTS films were done by senior reseach scientist of the Institute of Materials and Environmental Technology Dr. Jaan Raudoja. The six CZTS targets were synthesized from powders of binary compound metal sulfides, CZTS monograin powders or from powders of elements.

The first target was prepared from powders of metal sulfides. $Cu_2S$, ZnS and $SnS_2$ powders with the molar ratio of 1:1:1 were mixed and pressed into a pellet. Then the pellet was sealed into an evacuated quartz ampoule and heated at 900 °C for 48 h and then cooled to 500 °C for 150 h in a furnace. After that, the pellet was cooled to the room temperature. The third used target was done similarly $Cu_2S$, ZnS and $SnS_2$ powders as precursors were mixed, pressed into pellet, sealed into an ampoule and heated at 900 °C for 100 h and then at 720 °C for 12 h.

The second, fourth and fifth target were made from CZTS monograin powders. The size of powder crystals used in the second target was less than 38 μm or more than 112 μm. Sintering of pellets was made stepwise: at 700 °C for 36 h, and then at 900 °C for 50 h and finally at 100 °C for 10 h. The fourth target was made from CZTS monograin powder crystals, with size less than 38 μm. The powder was etched with 10% KCN solution before pressing into pellet.. Sintering was done at 900 °C for 100 h followed by heating at 720 °C for 50 h. The fifth target was made from a CZTS monograin powder with addition of sulphur. Pressed sample was heated at 500 °C for 50 h, cooled to the room temperature and S was removed from the ampoule. Then, the ampoule was heated at 900 °C for 400 h followed by heating at 700 °C for 24 h.

The sixth target was made using powders of Cu, Zn and Sn, and crushed them with S. From this mixture polycrystalline CZTS was synthesized by heating in a sealed vacuum ampoule at 500 °C for 24 h. Then temperature was slowly raised to 700 °C and kept constantly for 10 h.

After that, the poly-CZTS was crushed and heated again at 900 °C for 170 h followed by heating at 550 °C for 72 h.

## 2.5 Preparation of CZTS films

CZTS films were deposited by PLD (**Fig. 2.4**) onto 36.5×36.5 mm Mo/glass substrates. Before deposition, the substrates were cleaned ultrasonically in methanol and de-ionized water for 10 min at 50 °C for each steps. And then, the substrates were dried under nitrogen flow. The 18 mm in diameter target was fixed on a rotating target holder with rotation of 100 deg/s and the distance between target and substrate was 9 cm. A KrF excimer laser (Coherent Compex 102 F) with 248 nm was focused on a spot with an approximate area of 5 mm$^2$ on the surface of the rotating target. A pressure of $3 \times 10^{-6}$ Torr was maintained in the vacuum chamber.



**Fig.2.4** Pulsed laser deposition system

The properties and thickness of CZTS films were defined by the conditions of preparation of the CZTS films: the substrate temperature, laser wavelength (248 nm), laser energy density, pulse energy and the number of pulses and other parameters given in **Table 2.1.**

In the present studies the CZTS films properties as dependent on substrate temperature were studied in details.

**Table 2.1 Conditions for preparation of the CZTS films**

| No | target | substrate | $T_{substrate}$ (°C) | $E_{laserpulse}$ (mJ) | Number of pulses | Frequency( Hz) | $T_{anneal}$ (°C) | Cooling rate/ (°C/min) |
|---|---|---|---|---|---|---|---|---|
| 1 | NMS-04-15 | glass/Mo | 100 | 314 | 115000 | 6 | 400 | - |
| 2 | NMS-04-15 | glass | 100 | 300 | 115000 | 6 | 400 | - |
| 3 | NMS-04-15 | glass/Mo | 100 | 256 | 130000 | 7 | 450 | 5 |
| 4 | NMS-04-15 | glass | 300 | 300 | 115000 | 6 | - | 5 |
| 5 | NMS-09-15 | glass/Mo | 350 | 260 | 130000 | 7 | - | 5 |
| 6 | NMS-04-15 | glass/Mo | 400 | 260 | 130000 | 7 | - | 5 |
| 7 | NMS-09-15 | glass/Mo | 450 | 260 | 130000 | 7 | - | 5 |

## 2.6 KCN etching and selenization

The CZTS films deposited by PLD are crystalline, but not sensitive to light, as is expected at p-type semiconducting material. The use of annealing in different atmospheres can improve the chemical composition of the films and improve the PV properties of the film. Thus, CZTS films obtained by PLD method need to selenization or sulfurization treatment [71, 72].

In order to remove CuS and $Cu_2S$, CZTS films were etched with 10% KCN+1% KOH solution. Then the films were rinsed with ultrapure DI water and dried in nitrogen. In the present study we investigated the influence of selenization process to the properties of PLD deposited CZTS films. The selenization process, was performed in a quartz tube pumped down to $2 \times 10^{-2}$ Torr vacuum. $SnSe_2$ was used as Se source and as the component to suppress the decomposition of CZTS compound. . Selenization of CZTS was carried out in evacuated ampoules at 520 °C for 20 min and after that the ampoules were naturally cooled down to room temperature.

# 3. Results

## 3.1 Targets

Before depositing CZTS films, the first step was to prepare the targets. **Fig.3.1** shows the typical PLD target which was made from CZTS monograin powder. **Table 3.1** and **Fig.3.2** show the chemical compositions and SEM images of CZTS targets used in PLD method.



**Fig. 3.1** Typical Ø18 mm PLD target, sintered from CZTS monograin powder.

**Table 3.1 Composition of CZTS target**

| | Concentration of elements in CZTS target | | | | |
|---|---|---|---|---|---|
| No of target | Cu (at%) | Zn (at%) | Sn (at%) | S (at%) | Secondary phases |
| 1. | 24.47 | 11.32 | 13.29 | 48.64 | SnS |
| 2. | 27.89 | 13.57 | 14.42 | 44.12 | Sn |
| 3. | 24.67 | 11.41 | 15.45 | 48.47 | SnS, ZnS |
| 4. | 22.76 | 12.97 | 13.66 | 50.6 | SnS |
| 5. | 23.16 | 14.48 | 12.36 | 50 | Sn |
| 6. | 25.28 | 12.31 | 12.36 | 50.05 | CuS |

**Fig 3.2a** shows that the first target is inhomogeneous. The bright areas mark the secondary phase SnS and there is a small amount of selenium in the film. **Fig 3.2b** shows an inhomogeneous composition. The second target is copper-rich and sulfur-poor by EDX data. The bright areas mainly contain tin. **Fig 3.2c** shows that the third target is not homogenous. The secondary phases SnS and ZnS are present and there are ternary phases which consist of Cu, Sn and S in this sample
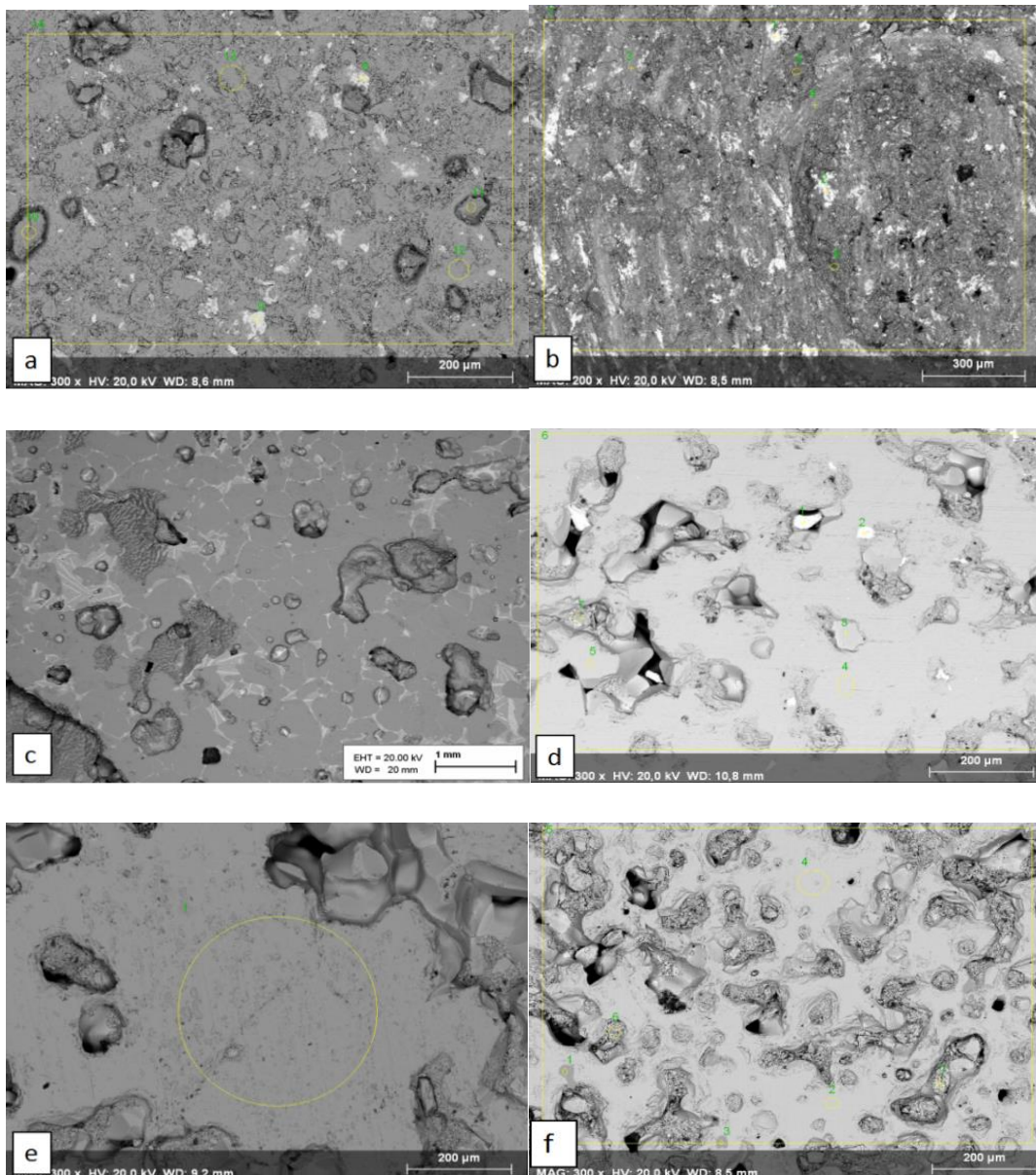


**Fig.3.2** SEM images of different CZTS targets

 **Fig 3.2d** shows that there are some small voids in this target. This target is slightly copper-poor and SnS phases are observed in the sample. But mainly the target is built up as single phase material. **Fig 3.2e** shows that the fifth target is relatively homogeneous. The chemical

composition of this target is slightly copper-poor and zinc-rich. **Fig 3.2f** shows that some voids are in the sixth target. A small amount of CuS phase is present.

In the present study fourth and fifth targets were used in CZTS films preparation.

## 3.2 Structure of PLD films

### 3.2.1 Surface structure of the PLD films

To study the influence of substrate temperature on CZTS structure, a series of films in temperature interval 300 - 450 °C were prepared. The SEM images of CZTS films for various substrate temperatures is shown in **Fig 3.3**. It is seen that, all samples have dense and compact morphologies without any obvious cracks or voids. The grains in CZTS films arranged with an average size of 200 nm at 300 °C **(Fig.3.3, a)**.
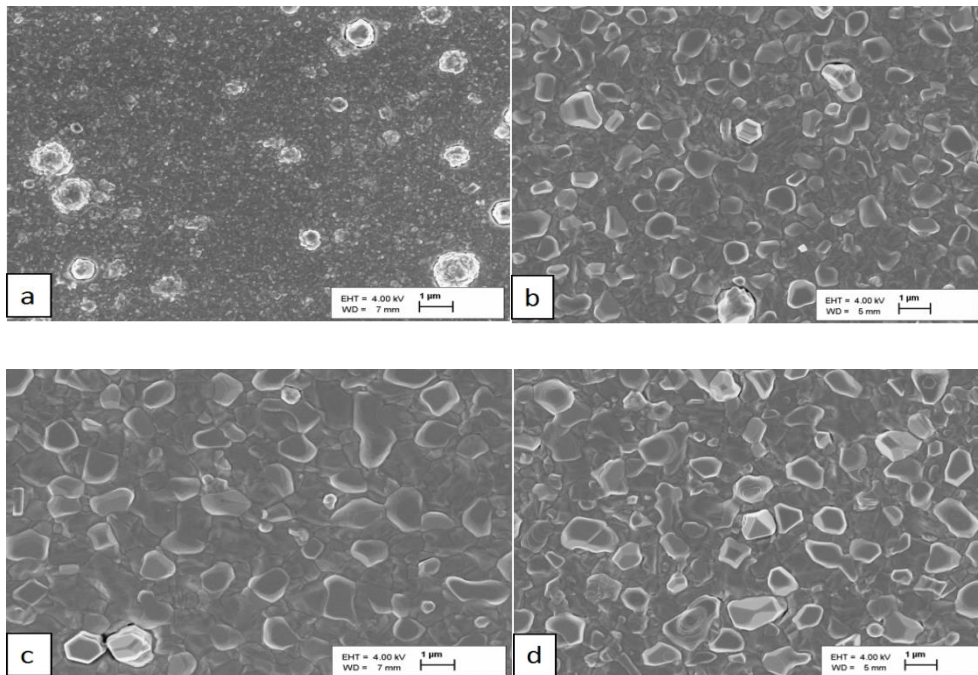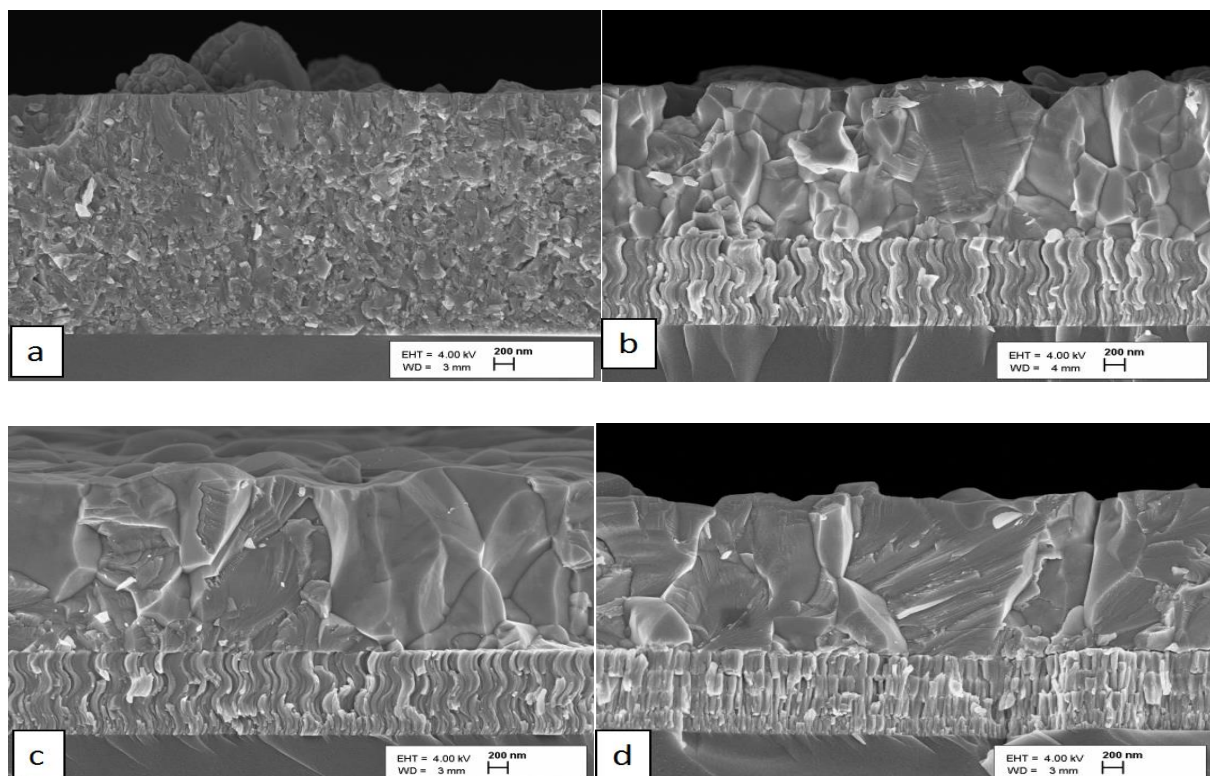


**Fig.3.3** SEM images of CZTS thin films deposited at different substrate temperatures: (a) 300 °C, (b) 350 °C, (c) 400 °C and (d) 450 °C

And some large particles can be observed in the film. The formation of large particles is probably attributed to the low mobility of deposited atoms on substrate at low temperature. Therefore, the crystalline quality need to be optimized. From 300 °C to 400 °C, the grains get significantly larger with increase in substrate temperature. The average grain size of the films grown at 350 °C (**Fig.3.3, b**) and 400 °C (**Fig.3.3, c**) are 500 nm and 1μm respectively. Increasing substrate temperature can improve the crystallinity and uniform of films. However, with the further increase of substrate temperature up to 450 °C (**Fig.3.3, d**), the grain size is not significantly increased in comparison with the previous films. On the same time obtained film is not more uniform and some holes - short circuit areas are presented in the film.

## 3.2.2 Cross-sectional structure of the PLD films

The cross-sectional SEM images of CZTS thin films for various substrate temperatures are presented in the Figure 3.4. It is seen that the substrate temperatures have an effect on the thickness of films.



**Fig.3.4** Cross-sectional SEM images of CZTS thin films for various substrate temperatures: (a) 300 °C, (b) 350 °C, (c) 400 °C and (d) 450 °C

**Fig.3.4,a** shows that the film with the thickness of approximately 3 μm was obtained at 300 °C. When the substrate temperatures was raised, the thickness of films decreased and trend to 2 μm at 450°C (**Fig.3.4,b-d**).

The cross-sectional SEM images also shows that the films are compact and dense. At 300 °C (**Fig.3.4,a**), some large particles and few holes on the top of the layer are seen. With the rise of substrate temperature, the number of larger particles decreases and the size of the holes get smaller near the top of the layer (**Fig.3.4, b-d**). Therefore, in the reasonable temperature range, increasing temperature can provide the thinner and more uniform films.

### 3.2.3 Grain size-temperature and thickness-temperature plots

**Fig.3.5a** shows the relationship between grain size and temperature. Before 400 °C, the crystal grains grow up rapidly by the temperature raising. After that, the grains' size increases slowly. **Fig.3.5b** shows the relationship between thickness and temperature. The thickness of film at initial temperature is 3μm. With the increase of temperature, the thickness is stabilized around 2μm.
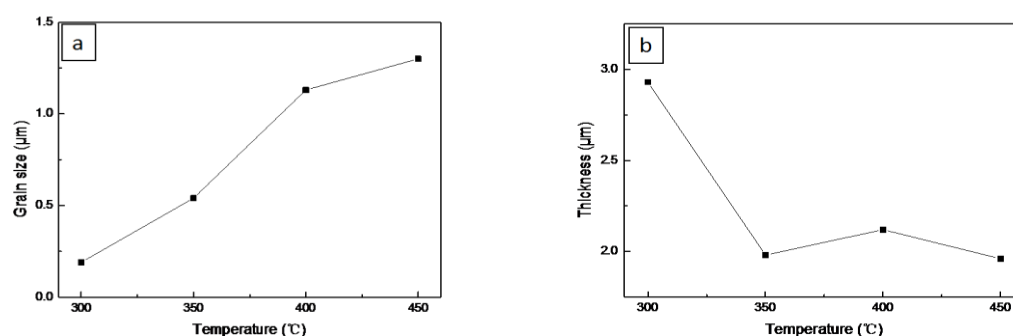


**Fig.3.5** (a). The relationship between grain size and temperature, (b) The relationship between thickness and temperature.

### 3.2.4 Summary and Discussion

The substrate temperature have the effect on film structure. Higher temperature results in the larger crystals. At 450 °C, the average size of CZTS crystal is 1.3μm. Higher temperature causes the thinner films, the thickness decreases from initial 3μm to 2μm.

## 3.3 Composition of the deposited PLD films

### 3.3.1 Chemical composition of the PLD films

In order to remove the secondary phases, the films were etched by KCN solution. **Table 3.2** shows the chemical composition before and after KCN treatment. Obviously, Cu content is decreased after KCN treatment. The Cu/(Zn+Sn) ratio of the as-deposited films is 1.18, 1.31, 1.54 and 1.64 at 300 °C, 350 °C, 400 °C, 450 °C respectively while the ratio of KCN etched films is 0.95, 0.99, 0.93 at 350 °C, 400 °C, 450 °C, respectively. These results indicate that Cu component increases with increasing temperature in as-deposited films. Moreover, KCN treatment effectively removes the secondary phases which are based on Cu. The Zn/Sn ratio of as-deposited films at 300 °C, 350 °C, 400 °C, 450 °C is 0.82, 0.87, 0.95 and 1.11 respectively. For the KCN etched films, the Zn/Sn ratio at 350 °C, 400 °C, 450 °C is 0.90, 0.91 and 1.05 respectively. This illustrates that the relative Zn content increases when the temperature increases. In addition, KCN treatment increases the relative Zn content.

**Table 3.2 Composition of the as-deposited and KCN etched films**

| Substrate temperature/treatment | Cu (at%) | Zn (at%) | Sn (at%) | S (at%) | Cu/(Zn+Sn) | Zn/Sn |
|---|---|---|---|---|---|---|
| 300 °C as-deposited film | 27.62 | 10.55 | 12.90 | 48.93 | 1.18 | 0.82 |
| 350 °C as-deposited film | 29.32 | 10.38 | 11.98 | 48.32 | 1.31 | 0.87 |
| 350 °C KCN etched film | 24.38 | 12.19 | 13.48 | 49.95 | 0.95 | 0.90 |
| 400 °C as-deposited film | 32.59 | 10.31 | 10.85 | 46.25 | 1.54 | 0.95 |
| 400 °C KCN etched film | 24.84 | 11.98 | 13.17 | 50.01 | 0.99 | 0.91 |
| 450 °C as-deposited film | 31.63 | 10.15 | 9.13 | 49.08 | 1.64 | 1.11 |
| 450 °C KCN etched film | 24.09 | 13.30 | 12.67 | 49.93 | 0.93 | 1.05 |

## 3.3.2 Crystals in as-deposited films

**Fig.3.6** shows the SEM images of as-deposited films for various temperatures. Phase composition was calculated on the basis of EDS element analysis results and percentage of phase consistency was calculated from SEM images by the help of image analysis methods. At 350 °C, the as-deposited film contains approximately 20% CuS, 3% $Cu_2S$ and 77% $Cu_2ZnSnS_4$ **(Fig.3.6, a)**. At 400 °C, the as-deposited film contains 40% CuS, and 60% $Cu_2ZnSnS_4$ **(Fig.3.6, b)**. At 450 °C, the as-deposited film contains 3% CuS, 40% $Cu_2S$ 3% and 57% $Cu_2ZnSnS_4$ **(Fig.3.6, b)**.
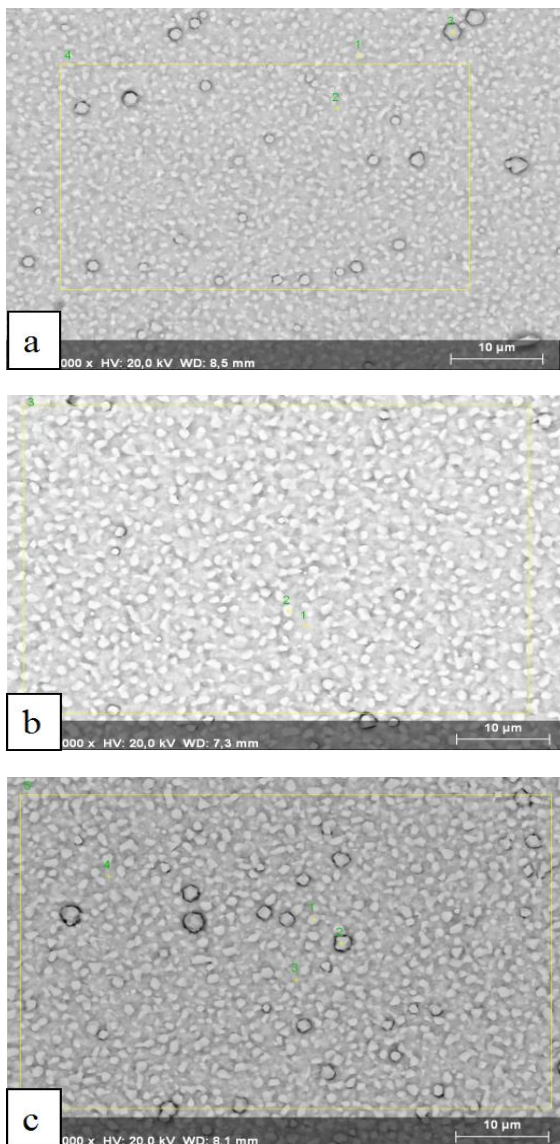


**Fig.3.6** SEM images of as-deposited films for various substrate temperatures: (a) 350 °C, (b) 400 °C and (c) 450 °C

### 3.3.3 Crystals in KCN etched films

KCN treatment removes the non-desirable phases – CuS or $Cu_2S$ from the films' structure.
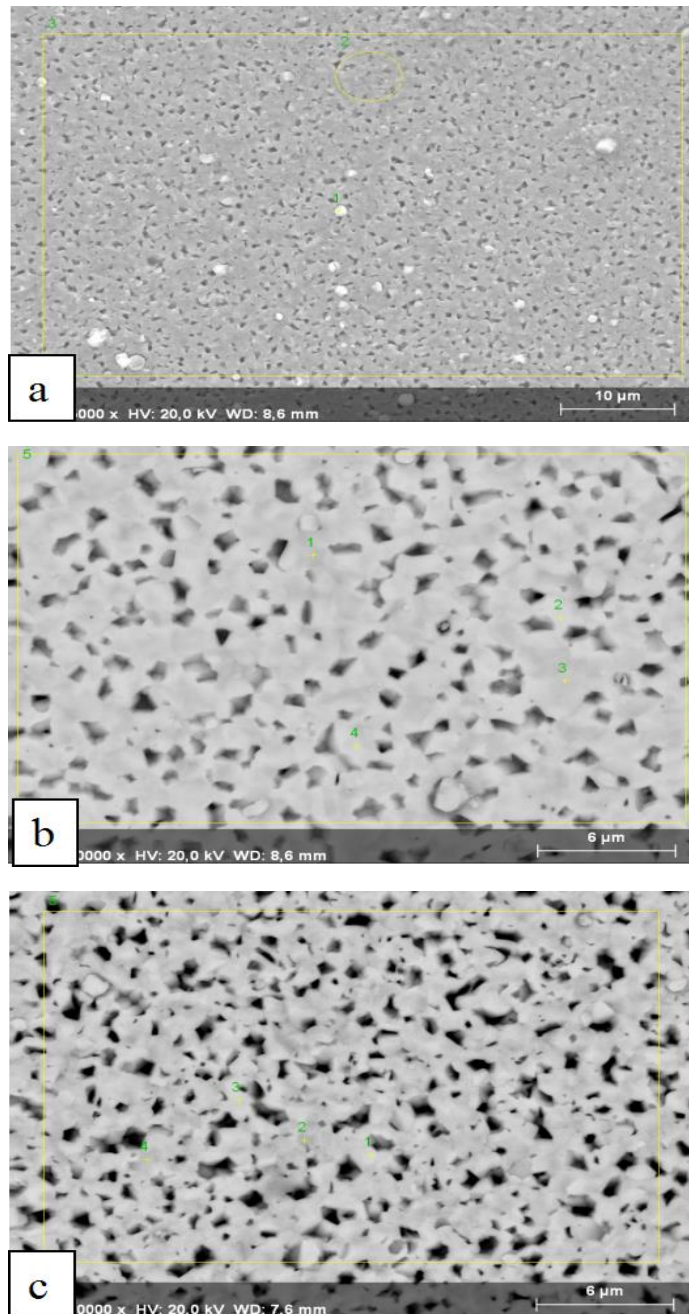


**Fig.3.7** SEM images of KCN etched films for various substrate temperatures: (a) 350 °C, (b) 400 °C and (c) 450 °C

**Fig.3.7** shows the SEM images of the remaining single phase films after KCN etching at various temperatures. At 350 °C, the etched film contains approximately 6% of $Cu_2ZnSnS_4$ large crystals and 94% $Cu_2ZnSnS_4$ as sintered target material **(Fig.3.7, a)**. At 400 °C and

450 °C, the etched films contain 100% of $Cu_2ZnSnS_4$ crystals with similar size are heavily joined to each other **(Fig.3.7, b and c)**.


### 3.3.4 Summary and discussion of the PLD film composition


The theoretical stoichiometry of CZTS is Cu:Zn:Sn:S = 2:1:1:4. However, most of the films have non-stoichiometrical composition. The composition of the films have an effect on the formation of secondary phases. The common secondary phases are CuS, $Cu_2S$, ZnS, SnS, $SnS_2$ and $Cu_2SnS_3$. In general, in the case of Cu-poor and Zn-rich films, effective photo-absorber layers can be prepared.

To study the influence of temperature on the composition of the films, the films deposited at 300 °C, 350 °C, 400 °C and 450 °C were analyzed. For the as-deposited films, the ratio of Cu/(Zn+Sn) changes from 1.2 to 1.6 when the temperature changes from 300 °C to 450 °C. It means that all the analyzed as-deposited films are Cu-rich. And increase of the temperature gives increase of the copper content. The ratio of Zn/Sn is in the range from 0.8 to 1.1 for the temperature range from 300 °C to 450 °C. It indicates that the films trend to be Zn-rich with increasing of temperature. In addition, the type of the secondary phases changes at different temperature. At 350 °C and 400 °C, the main secondary phase in the as-deposited films is CuS and the proportion of CuS at 400 °C is higher than that at temperature of 350 °C. At 450 °C, the main secondary phase in the as-deposited film is $Cu_2S$.

The formation of secondary phases in photo-absorber layer can reduce the solar cell efficiency, therefore it is necessary to remove the secondary phases from the CZTS films. In this thesis, KCN etching treatment was used for removing the CuS and $Cu_2S$ phases. Compared with the as-deposited films, the Cu/(Zn+Sn) ratio of KCN etched films is reduced and all the ratios are less than 1. It means that the KCN treatment results in the films from Cu-rich to Cu-poor depending on temperature. At 350 °C, the etched film contains few $Cu_2ZnSnS_4$ large crystals while for the substrate temperature of  400 °C and 450 °C, the films are homogenous and all the secondary phases are removed. However, KCN etching leads to the formation of the number of voids in the films which can be the potential areas for short circuit of the PV-element.

## 3.4 Selenization of the PLD films

## 3.4.1 Selenization of the as-deposited films

Despite the structure and composition of the deposited at 350 - 450 °C films were close to ideal - 2 μm thick, large crystals through the film in the form of columnar structure, composition close to the stoichiometric, the films PV response was very low. Therefore, obtained CZTS films needed to be activated. Usually some chemical or thermal treatments were performed. In the case of $Cu_2ZnSnS_4$ films usually S or Se treatment at higher temperature is performed. In our study we tried to make a selenization of the films.
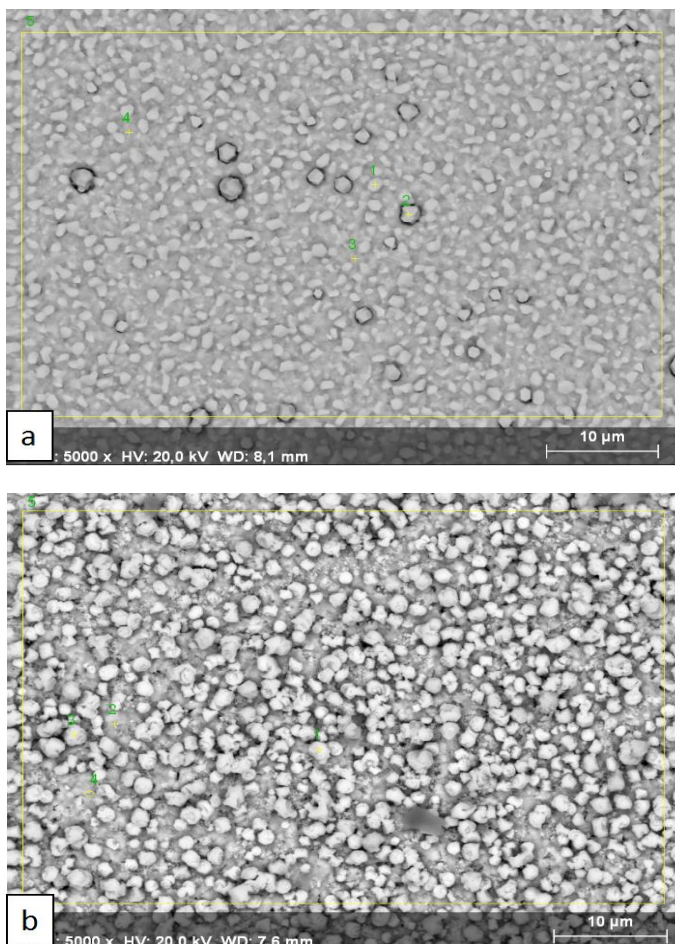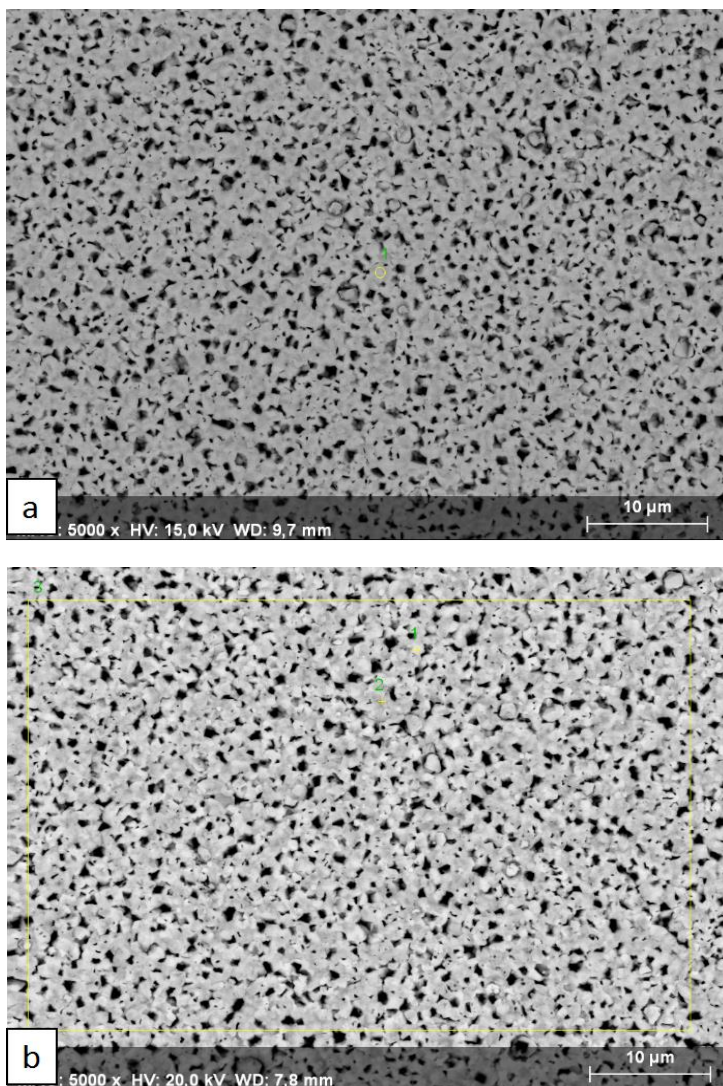


**Fig.3.8** SEM images of as-deposited films : (a) as-deposited film before selenization , (b) deposited film after selenization

43

**Fig.3.8** shows SEM images of the deposited film before and after selenization. Before selenization (**Fig.3.8a)**, the large number of $Cu_2S$ crystals are in the film structure, with the size about 1 μm. After selenization (**Fig.3.8b)**, the large number of 1.5 μm white crystals are observed in the film, which contain copper, tin, sulfur and selenium.

## 3.4.2 Selenization of the KCN etched film

**Fig.3.9** shows the KCN etched film images before and after selenization at 520 °C for 20 min.



**Fig.3.9** SEM images of KCN etched films: (a) KCN etched film before selenization , (b) KCN etched film after selenization

It is seen that the KCN etched film is homogeneous due to $Cu_2S$ and $CuS$ phases are removed (**Fig.3.9a**). Hence, the KCN etched film are without secondary phases after selenization (**Fig.3.9b**).

### 3.4.3 Composition of selenized films

**Fig.3.10** shows the EDX spectra of the films and the compositional results are shown in **Table 3.3**. Selenization of the films results in the fact that a part of sulfur is replaced by selenium. The as-deposited film is Zn-poor. Nearly half of the sulfur in the as-grown layer is replaced by selenium after selenization while in the KCN etched films only 20% of the sulfur is replaced and the concentrations of other elements are close to the CZTS stoichiometry.
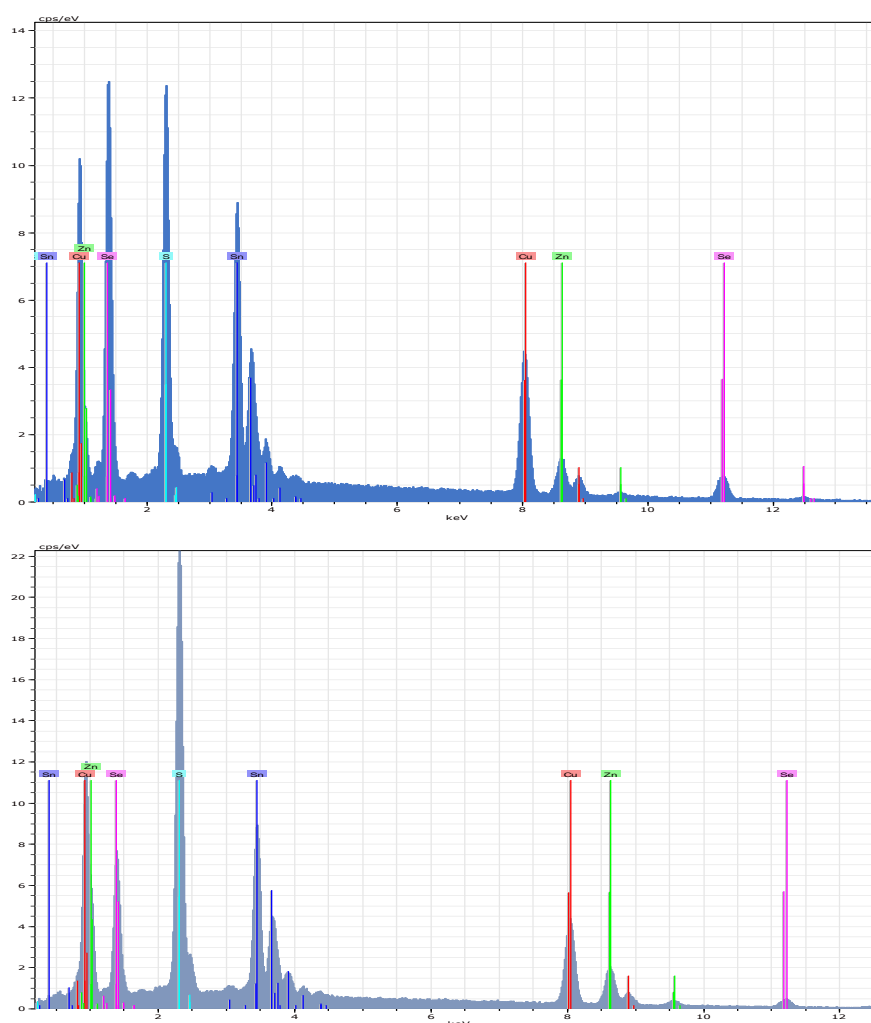


**Fig.3.10** EDX spectra of the films: (a) as-deposited film after selenization, (b) KCN etched film after selenization.

**Table 3.3 Composition of the selenized films deposited at 520 °C for 20 min.**

|  | Cu (at%) | Zn (at%) | Sn (at%) | S (at%) | Se (at%) |
|---|---|---|---|---|---|
| as-deposited film | 27.13 | 8.43 | 15.28 | 29.02 | 20.14 |
| KCN etched film | 23.36 | 12.69 | 13.39 | 40.34 | 10.22 |

## 3.4.4 Summary and discussion of selenization of films

Selenization is an approach to improve the performance of the films. To study the effect of selenization on structure and composition of the CZTS films, an as-deposited CZTS film and a KCN etched film were treated by selenization. High temperature promoted the reactionsbetween the film components and $SnSe_2$. The films were characterized by SEM and EDX.

The as-deposited films are Cu-rich, having a significant amount of $Cu_2S$ and little amount of CuS secondary phases. In the selenization process, these secondary phases reacted with $SnSe_2$ to produce a new secondary phase. The new secondary phase contains 30% copper, 5% zinc, 16% tin, 21% sulfur and 28% selenium. In addition, in the annealed film 50 % sulfur was replaced by selenium. However, relative content of Zn is obviously insufficient. This is probably due to Sn was added when the sulfur was replaced by selenium.

The $Cu_2S$ and CuS secondary phases were removed by KCN etching of film, so the film is compositionally homogeneous. In the selenization process, the components in CZTS film reacted with $SnSe_2$ to produce homogeneous CZTSSe through the film and 20% of the sulfur was replaced by selenium.

## 3.5 Photosensitivity of the PLD films

### 3.5.1 as-deposited film

The reason to study the applicability of Kelvin Probe method on $Cu_2ZnSnS_4$ films was to get fast answers about the PV characteristics of the prepared absorbers without preparing the complete solar cell. **Fig.3.11** shows the surface potential change in the dark and under red laser illumination for the as-deposited CZTS films before and after selenization. Both of them are not photosensitive (measurement accuracy +/- 5 meV).
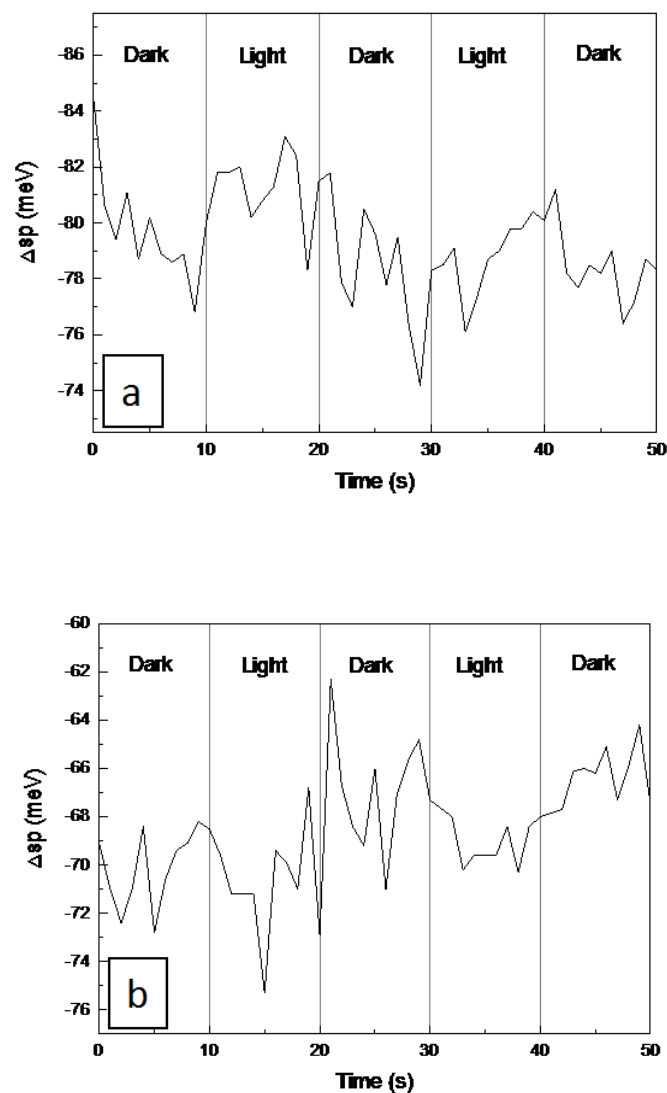


**Fig.3.11** Surface potential change in the dark and under red laser illumination for CZTS films: (a) as-deposited film before selenization , (b) as-deposited film after selenization

## 3.5.2 KCN etched film

**Fig.3.12** shows the surface potential change in the dark and under red laser illumination for the KCN etched CZTS films before and after selenization. The photosensitivity of them is not good. The reasons for poor photosensitivity is not clear so far and need to be investigated in future.
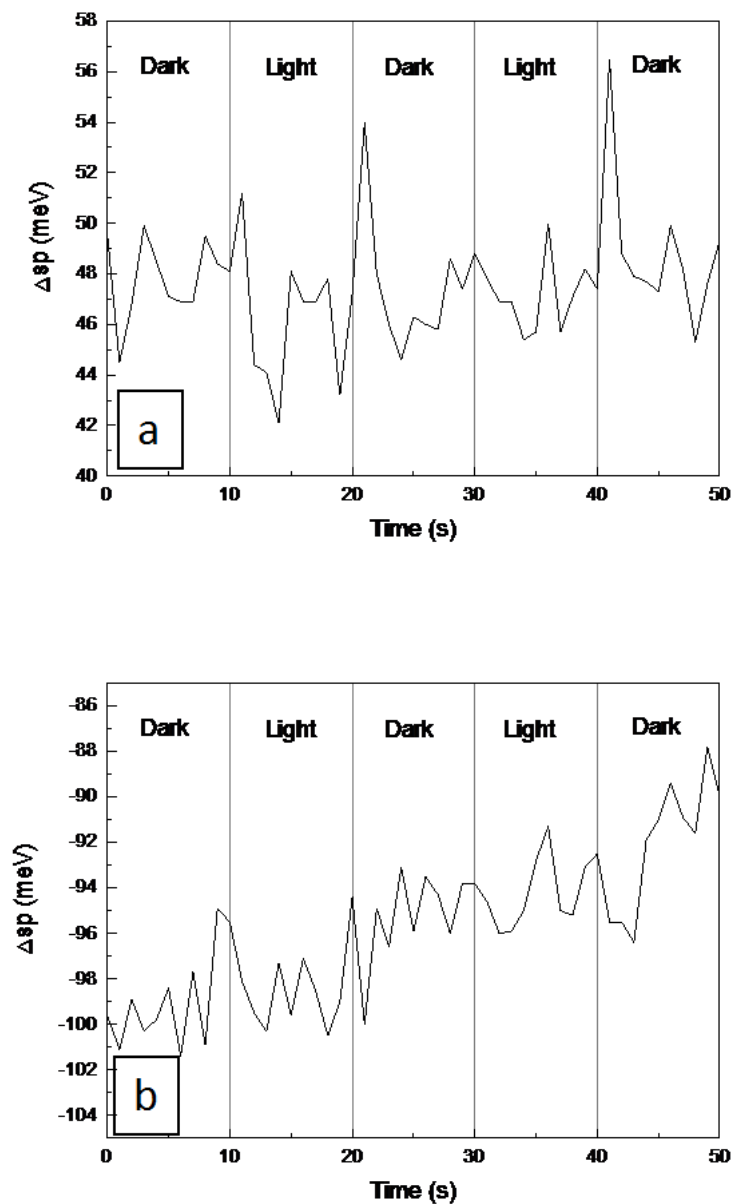


**Fig.3.12** Surface potential change in the dark and under red laser illumination for CZTS films: (a) KCN etched film before selenization , (b) KCN etched film after selenization

### 3.5.3 Summary and discussion

To study the effect of selenization on the photosensitivity of CZTS films, the Kelvin Probe was used for measuring the surface potential change for the four samples: as-deposited film before and after selenization, KCN etched film before and after selenization. However, the results show that the films after selenization at 520 °C for 20 min did not improve the photosensitivity.

Combined with the structure and composition of selenized films which were described in Chapters 3.2 and 3.3, we can analyze the reason why the films selenized at 520 °C for 20 min did not get good performance in photosensitivity.

For the as-deposited film, the layer has the large number of secondary phases: CuS and $Cu_2S$. In this case, selenization cannot remove these secondary phases which result in low efficiency. On the contrary, selenization leads to form new secondary phases. Hence, the composition is not optimal.

For the KCN etched film, all of the secondary phases were removed from the film. After selenization the film composition was 23.36% Cu, 12.69% Zn, 13.39% Sn, 40.34% S, 10.22% Se - 20% of the S was replaced by Se. The results of Kelvin Probe measurement indicate that selenization at 520 ℃ for 20 min didn't improve the films sensitivity to light. Some additional thermal or chemical treatments are needed. To the future studies a thermal treatment in sulphur atmosphere can be helpful.

# 4. Conclusions

1. A number of uniform CZTS targets for PLD have been prepared by sintering and series of CZTS thin films has been deposited by PLD onto glass and glass/Mo substrates at different substrate temperatures.

2. The grain size of CZTS films increases with increasing of substrate temperature and 1.3 μm crystals were achieved at 450 °C. High temperature improves the uniformity of obtained CZTS films. At temperatures 400 °C and 450 °C large grains grow through the films as observed and obtained films have columnar structure.

3. The thickness of CZTS films decrease by increasing of substrate temperature. The thickness of the film at substrate temperature 300 °C was 3 μm and at the temperature range of 350-450 °C was 2 μm.

4. At all used substrate temperatures the obtained films consist of 2 phases – $Cu_2ZnSnS_4$ matrix phase and $Cu_xS$ phase. Thereby the PLD deposited CZTS films were Cu-rich with tendency to increase copper content with increasing temperature.

5. The composition of formed secondary phase in films changes at higher used substrate temperatures: at 350 °C and 400 °C, the main secondary phase in the as-deposited films is CuS, at 450 °C, the main secondary phase in the as-deposited film is $Cu_2S$.

6. KCN etching removes the CuS and $Cu_2S$ phases from the deposited films. There are large number of holes in the films after KCN treatment.

7. Thermal selenization results in the partial replacement of sulfur by selenium. For as-deposited film, 50% of the CZTS surface region sulfur is replaced by selenium. The selenization of previously KCN etched films showed homogeneous composition through the film and 20 % sulfur is replaced by selenium.

8. Selenization at 520 °C for 20 min did not improve the photosensitivity of as-deposited and KCN etched films.

# Résumé

The present thesis is devoted to the study the $Cu_2ZnSnS_4$ films prepared by PLD. Main attention is devoted to investigate the structure, composition, and electrical properties of the films. It is difficult to deposit single phase CZTS, the secondary phases form much easier than single phase CZTS during PLD process. In order to obtain high performance films, the condition of deposition and annealing treatment should be optimized. Chapter 1 gave an introduction of photovoltaic basics, solar cell efficiency, and thin film technologies. In the end of the chapter the aim of the present thesis is given. Chapter 2 introduced the apparatus of analyzing the structure and composition, deposition condition and selenization method. Chapter 3 introduce the preparation of target and gave the results of the investigations of films structure and composition.

All films were deposited from CZTS targets, which are made from monocrystalline single phase powder by sintering method. To study the effect of temperature on the structure of CZTS film, the films were deposited at 300 °C, 350 °C, 400 °C, 450 °C. The results show that higher temperature cause larger grain size and thinner films. At 450 °C, the grain size and thickness are 1.3 μm and 2 μm respectively. At higher temperatures films show columnar structure.

To study the effect of temperature on the composition of CZTS film, the films were analyzed by EDX. The results show that all the as-deposited films are multiphase and Cu-rich and the Cu content increasing with the temperature increase. There are secondary phases of CuS and $Cu_2S$ in the resulted films. At 350 °C and 400 °C, the main secondary phase is CuS. At 450 °C, the main secondary phase is $Cu_2S$.

In order to remove the secondary phases, the films were treated by KCN etching. The KCN etching proceeded very rapidly and after etching all $Cu_xS$ phases were removed from films structure. The results show that the KCN etching can remove all of the CuS and $Cu_2S$. In addition, there are lot of pores in etched films. Usually the pores are on the top of films and didn't penetrate through all the film thickness.

The selenization of films were carried out in furnace at 520 °C for 20 min. After selenization and etching, 20% of sulfur was replaced by selenium. However, the results of Kelvin Probe

measurements show that selenization at 520 °C for 20 min did not improve the photosensitivity.

# RESÜMEE

Käesolev magistritöö on pühendatud $Cu_2ZnSnS_4$ (CZTS) optoelektroonsete kilede uurimisele mis sadestatud pulseeriva kiirega lasersadestamise (PLD) meetodil. Peatähelepanu on pööratud kilede struktuuri, koostise ning elektriliste ja optiliste omaduste uurimisele. Üldiselt on teada, et monofaasilise CZTS kile sadestamine on komplitseeritud ning tavaliselt lisanduvad sadestamisel kilede struktuuri mitmed sekundaarsed ning samas mittesoovitud faasid. Et saada soovitud koostise ja omadustega kilesid tuleb nende sadestamise ning hilisema töötluse protsesse sügavuti uurida ning optimeerida. Käesolevas töös on kilede sadestamisel kasutatud PLD meetodit. Teoreetiliselt peaks see meetod võimaldama keeruka koostisega materjali ülekandmist märklaualt sadestusalusele.

Praktikas osutusid (sõltumata PLD parameetritest) saadud kiled kahefaasilisteks, koosnedes märklaua materjalist- $Cu_2ZnSnS_4$ ning $Cu_xS$ faasist.

Esimeses peatükis antakse kirjanduse ülevaade tänapäeva hetkeseisust optoelektroonika rakendustes, peamiste päikesepaneelide materjalidest, tehnoloogiatest ning saavutatud efektiivsustest. Peatüki lõpus on ära toodud antud magistritöö peamised eesmärgid. Teises peatükis kirjeldatakse töös kasutatud aparatuurseid meetodid ning kilede sadestamise ja töötlemise karakteristikuid. Kolmandas osas antakse ülevaade saadud tulemustest.

Kuna töö peamine uudsus on seotud ühefaasilistest monokristallidest kokkupaagutatud PLD märklaua abil saadud CZTS kilede uurimisega, siis on töös eraldi välja toodud ülevaade teiste uurimisgruppide poolt kasutatud märklaudadest ning kohapeal valmistatud märklaudade tehnoloogiast. Uurimaks kilede omaduste sõltuvust temperatuurist sadestati samadel algtingimustel CZTS kiled erineva temperatuuriga Mo-klaasile. Temperatuurid olid 300, 350, 400 ja 450 °C. Vastavalt saadud tulemustele oli näha, et aluse temperatuuri tõustes kilede terad suurenesid. Samas muutus kile õhemaks (3 μm - 2 μm) ning kompaktsemaks. Temperatuuridel 400-450 °C pihustatud kiled omasid kolonnilist struktuuri ning kristalliterad olid kasvanud läbi kile. 450 °C juures sadestatud kile paksus oli 2 μm ja terade keskmine suurus 1.3 μm.

Kilede koostise uurimiseks sõltuvalt sadestamise temperatuurist kasutati energiadispersiivse röntgenmikroanalüüsi meetodit- EDX. Vastavalt saadud tulemustele olid kõik sadestatud kiled mitmefaasilised ja vaserikkad ning vase sisaldus kasvas sadestamistemperatuuri tõstmisega. Lisaks märklaua faasile (nn. maatriks - $Cu_2ZnSnS_4$), sisaldasid saadud kiled CuS

või Cu$_2$S faasi. 350 ja 400 °C juures sadestatud kiled omasid lisaks maatriksile peamiselt CuS ning 450 °C sadestatud kiled Cu$_2$S faasi.

Eemaldamaks kiledest Cu$_x$S faasi söövitati neid KCN lahuses. Söövitusprotsess toimus äärmiselt kiiresti ning juba 1 sekundiline söövitus eemaldas kilede struktuurist kõik sekundaarsed faasid. Tulemuseks olid ühefaasilised ning küllaltki poorsed kiled. Vaatamata suurele poorsusele ei olnud poorid tavaliselt kile läbivad.

Kilede seleniseerimine toimus ahjus 520 °C juures 20 minuti jooksul. Peale seleniseerimist oli 20 % väävlist kile koostises asendunud seleeniga. Siiski, vastavalt nn. Kelvin Probe meetodile ei olnud seleniseeritud kilede optoelektroonsed omadused märkimisväärselt paranenud ning selle eesmärgi saavutamiseks tuleks kasutada teisi termilisi ja keemilisi meetodeid, näiteks väävlitöötlust, erinevat termilist käsitlust või siis muuta märklaua koostist.

# REFERENCES

[1] R. Williams (1960). Becquerel Photovoltaic Effect in Binary Compounds. The Journal of Chemical Physics. 32 (5): p. 1505–1514.

[2] E. Becquerel (1839). "Mémoire sur les effets électriques produits sous l'influence des rayons solaires". Comptes Rendus. 9: p. 561–567.

[3] https://en.wikipedia.org/wiki/Theory_of_solar_cells

[4] P.S. Priambodo, N.R. Poespawati, D. Hartanto. (2002) "Chapter book: Solar Cell Technology", INTECH Open Access Publisher.

[5] L. M. Peter. (2014) "Electrochemical routes to earth-abundant photovoltaics: A minireview "Electrochemistry Communications Vol. 50, January 2015, p. 88–92.

[6] S. Rühle. (2016) Tabulated Values of the Shockley-Queisser Limit for Single Junction Solar Cells. Solar Energy. 130: 139–147.

[7] M. A. Green (2003). Third Generation Photovoltaics: Advanced Solar Energy Conversion. Springer. p. 65.

[8] https://www.nrel.gov/pv/assets/images/efficiency-chart.png.

[9] Poortmans J, Arkhipov V. Thin Film Solar Cells: Fabrication, Characterization and Applications[M]. John Wiley & Sons, Ltd, 2006.

[10] S. G. Kumar and K. S. R. Koteswara Rao. (2014) Physics and chemistry of CdTe/CdS thin film heterojunction photovoltaic devices: fundamental and critical aspects. Energy Environ. Sci., 7, p. 45-102.

[11] S.R. Wenham, M.A. Green, M.E. Watt, R. Corkish. (2007) Applied Photovoltaics, Earthscan, 2007, Chapt. 2.

[12] C. R. Wronski, et al. (2004) "Intrinsic and Light Induced Gap States in a-Si:H Materials and Solar Cells - Effects of Microstructure", Thin Solid Films, 451-452, p. 470-475.

[13] B.E.Mc Candless, J.R. Sites. (2005) Cadmium Telluride Solar Cells, in:Handbook of Photovoltaic Science and Engineering. John Wiley&Sons, Ltd., p.617– 662.

[14] W. Shockley,H.J. Queisser. (1961) Detailed balance limit of efficiency of p-n junction solar cells. J.Appl.Phys.32, 510.

[15] www.firstsolar.com. (2014) First Solar Sets Thin-Film Module Efficiency World Record of 17.0 Percent.

[16] J. H. Werner (2011). Toxic Substances in Photovoltaic Modules" (PDF). Post free market.net. Institute of Photovoltaics, University of Stuttgart, Germany - The 21st International Photovoltaic Science and Engineering Conference 2011 Fukuoka, Japan. p. 2.

[17] Solar, Inc. 2011.Water Solubility of Cadmium Telluride in a Glass-to-Glass Sealed PV Module" (PDF). Vitreous State Laboratory, and AMELIO

[18] V. Fthenakis, M. Fuhrmann, J. Heiser, W. Wang (2004). Experimental Investigation of Emissions and Redistribution of Elements in CdTe PV Modules during Fires. (PDF). 19th European PV Solar Energy Conference. Paris, France.

[19] S. Beckmann and L. Mennenga (2011). Calculation of emissions when there is a fire in a photovoltaic system made of cadmium telluride modules. Bavarian Environmental Protection Agency.

[20] T. Tinoco et al. (1991). Phase Diagram and Optical Energy Gaps for $CuIny Ga1-ySe_2$ Alloys. Physica Status Solidi (a). 124 (2): 427.

[21] P. Jackson, et al. (2016) Effects of heavy alkali elements in $Cu(In,Ga)Se_2$ solar cells with efficiencies up to 22.6%, Phys. Status Solidi (RRL) – Rapid Res. Lett.

[22] E. Yablonovitch et al. (2012) The opto-electronic physics that broke the efficiency limit in solar cells. 2012 38th IEEE Photovoltaic Specialists Conference. p. 001556.

[23] R. Nitsche, D. F. Sargent, P. Wild. (1967) Crystal Growth of Quaternary I(2)II-IV-VI (4) Chalcogenides by Iodine Vapor Transport. Journal of Crystal Growth. 1 (1): p. 52–53.

[24] H. Yoo, J. Kim. (2011) Comparative study of $Cu_2ZnSnS_4$ film growth. Solar Energy Mater. Solar Cells 95, p. 239–244.

[25] S.A. Vanalakar, et al. (2015) A review on pulsed laser deposited CZTS thin films for solar cell applications. J. Alloys Compd. 619, p. 109 -121.

[26] Z. Huanping et al. (2013) CZTS nanocrystals: a promising approach for next generation thin film photovoltaics. Energy Enviro. Sci., 6, p. 2822-2838.

[27]Tanaka,K,Oonuki, M,Moritake, N, Uchiki, H., 2009. Thin film solar cells prepared by non-vacuum processing. Sol. Energy Mater. Sol. Cells 93, 583–587.

[28] Chen S, Gong XG, Walsh A, Wei SH. Defect physics of the kesterite thin-film solar cell absorber Cu2ZnSnS4. Appl. Phys. Lett. 2010; 96: 021902

[29] I. D. Oleksyuk, I. V. Dudchar, L. V. J. Piskach. (2004) Journal of Alloys and Compound. 368, p. 135 -143.

[30] J.S., Seol et al. (2003) Electrical and optical properties of $Cu_2ZnSnS_4$ thin films prepared by RF magnetron sputtering process. Sol. Energy Mater. Sol. Cells 75, p. 155–162.

[31] J. Wang et al. (2013) $Cu_2ZnSnS_4$ thin films: facile and cost-effective preparation by RF-magnetron sputtering and texture control, J. Alloys Compd. 552, p. 418-422.

[32] K.A. Vinaya Kumar et al. (2014) simple chemical approach for the deposition of Cu2ZnSnS4thin films. physica status solidi (a),Vol 211, Issue 8, p. 857–1859.

[33] T. R. Rana, N.M. Shinde, J.H. Kim. (2016) Novel chemical route for chemical bath deposition of $Cu_2ZnSnS_4$ (CZTS) thin films with stacked precursor thin films. Materials Letters Volume 162, p. 40–43.

[34] K. Tanaka et al. (2009). $Cu_2ZnSnS_4$ thin film solar cells prepared by non-vacuum processing. Sol. Energy Mater. Sol. Cells 93, p. 583–587.

[35] G. Larramona et al. (2015) Fine-tuning the Sn content in CZTSSe thin films to achieve 10.8% solar cell efficiency from spray-deposited water–ethanol-based colloidal inks. Adv. Energy Mater. 5 (2015).

[36] K. Tanaka. (2012) Face-to-face annealing process of $Cu_2ZnSnS_4$ thin films deposited by spray pyrolysis method. Jpn. J. Appl. Phys. 51.

[37] A.V. Moholkar et al. (2011) Development of CZTS thin films solar cells by pulsed laser deposition: Influence of pulse repetition rate, Sol. Energy 85, p. 1354–1363.

[38] K. Moriya, K. Tanaka, H. Uchiki. (2007) Fabrication of $Cu_2ZnSnS_4$ thin film solar cell prepared by pulsed laser deposition. Jpn. J. Appl. Phys. 46, p. 5780–5781.

[39]C.W. Shi et al. (2012) Deposition of $Cu_2ZnSnS_4$ thin films by vacuum thermal evaporation from single quaternary compound source. Mater. Lett. 73, p. 89–91.

[40] K. Oishi et al. (2008) Growth of $Cu_2ZnSnS_4$ thin films on Si (1 0 0) substrates by multisource evaporation. Thin Solid Films 517, p. 1449–1452.

[41] K. Ito, T. Nakazawa (1988) Electrical and optical-properties of stannite-type quaternary semiconductor thin-films, Jpn. J. Appl. Phys. 1 (27), p. 2094–2097.

[42] J.J. Scragg, P.J. Dale, L.M. Peter. (2008) Towards sustainable materials for solar energy conversion: Preparation and photoelectrochemical characterization of $Cu_2ZnSnS_4$. Electrochem. Commun. 10, p. 639–642.

[43] A. Ennaoui et al. (2009) $Cu_2ZnSnS_4$ thin film solar cells from electroplated precursors: novel low-cost perspective, Thin Solid Films 517, p. 2511–2514.

[44] B. Ruggero et al. (2012) Surface Engineering for Bone Implants: A Trend from Passive to Active Surface Coatings. 2(3), p. 95-119

[45] N. Amin and K. S. Rahman (2017) Close- Spaced Sublimation (CSS): A Low- Cost, High- Yield Deposition System for Cadmium Telluride (CdTe) Thin Film Solar Cells,

Modern Technologies for Creating the Thin-film Systems and Coatings, Prof. Nikolay Nikitenkov (Ed.), InTech.

[46] Antonio L，Steven H (2011). Handbook of Photovoltaic Science and Engineering.

[47] Hodes G (2003) Chemical solution deposition of semiconductor films. Marcel Dekker, New York

[48] R. R. Chamberlin and J. S. Skarman. (1966) Chemical spray deposition process for inorganic films. Journal of the Electrochemical Society, 113(1), p. 86-89.

[49] L. Filipovic, Topography Simulation of Novel Processing Techniques(Dissertation), Technischen Universität Wien, Fakultät für Elektrotechnikund Informationstechnik, 2012

[50] Kai Wang (2013). Laser Based Fabrication of Graphene, Advances in Graphene Science, Dr. M. Aliofkhazraei (Ed.), InTech.

[51] Douglas B. Chrisey, Graham K.Hubler.(1976) Pulsed Laser Deposition of Thin Films. p. 167-168

[52] Douglas B. Chrisey, Graham K.Hubler.(1976) Pulsed Laser Deposition of Thin Films. p. 168-169

[53] Douglas B. Chrisey, Graham K.Hubler.(1976) Pulsed Laser Deposition of Thin Films. p. 294-295

[54] Douglas B. Chrisey, Graham K.Hubler.(1976) Pulsed Laser Deposition of Thin Films. p. 296-298

[55] Muska K, Kauk M, Altosaar M, et al. Synthesis of Cu2ZnSnS4 monograin powders with different compositions[J]. Energy Procedia, 2011, 10: 203-207.

[55] A.V. Moholkar et al. (2011) Synthesis and characterization of $Cu_2ZnSnS_4$ thin films grown by PLD: Solar cells Journal of Alloys and Compounds. 509 (2011) p. 7439–7444

[56] M. P. Suryawanshi et al. (2013) CZTS based thin film solar cells: a status review. Advanced Performance Materials, V28, I. 1-2. P. 347-351.

[57] A.V. Moholkar, et al. (2011) Development of CZTS thin films solar cells by pulsed laser deposition: Influence of pulse repetition rate. Semiconductor Materials for Solar Photovoltaic Cells. Springer.

[58] M. Kotani, et al. (2017) Composition-ratio control of CZTS films deposited by PLD. Phys. Status Solidi C 2017, 10.1002/pssc.201600212

[59] S. R. Kodigala. (2014) Thin Film Solar Cells From Earth Abundant Materials: Growth and Characterization of $Cu_2ZnSn(SSe)_4$ Thin films and Their Solar Cells. Elsevier eBook.

[60] L. Sun et al. (2011) Structure, composition and optical properties of $Cu_2ZnSnS_4$ thin films deposited by Pulsed Laser Deposition method. Solar Energy Materials and Solar Cells. 95, p. 2907-2913.

[61] M. von Ardenne (1937) Improvements in electron microscopes. GB 511204, convention date (Germany).

[62] I. M. Watt. (1997) The Principles and Practice of Electron Microscopy.

[63] J. Goldstein (1975). Practical Scanning Electron Microscopy: Electron and Ion Microprobe Analysis.

[64] P. J. Potts, J.F. Bowles, S.J. Reed, R. Cave. (1995) Microprobe Techniques in the Earth Sciences. Springer.

[65] X. Li et al. (2013) Detection of Lithium X-rays by EDS. Microsc. Microanal. 19 (Suppl 2), 2013

[66] Dieter K. Schroder. (2006) Semiconductor Material and Device Characterization.

[67] C. Li et al. (2015) (Bruker Nano Surfaces). Peak Force Kelvin Probe Force Microscopy.

[68] Bruker Nano Surfaces, High-Resolution, Quantitative Work Function Measurements with PeakForce Kelvin Probe Microscopy (KPFM)(2016)

[69] K. Baikie et al. (2000) Work Function study of rhenium oxidation using an ultra-high vacuum scanning Kelvin probe. Journal of Applied Physics, Vol. 88, p. 4371.

[70] I. D. Baikiea and P. J. Estrup. (1998) Low cost PC based scanning Kelvin probe, Rev. Sci. Instum. Vol 69.

[71] G. Surgina et all. (2013) Reactive pulsed laser deposition of $Cu_2ZnSnS_4$ films in $H_2S$. Thin Solid Films, 535, p.44-47.

[72] Nurul A. et all. (2015) The growth of nanostructured $Cu_2ZnSnS_4$ films by pulsed laser deposition. Applied Surface Science.